New Glycoconjugation Strategies for Ruthenium(II) Arene Complexes via Phosphane Ligands and Assessment of their Antiproliferative Activity

Dalila Iacopini,[a] Ján Vančo,[b] Sebastiano Di Pietro,[c] Vittorio Bordoni,[c] Stefano Zacchini,[d] Fabio Marchetti,[a] Zdeněk Dvořák,[e] Tomáš Malina,[b] Lorenzo Biancalana,[a,*] Zdeněk Trávníček,[b,*] Valeria Di Bussolo [c,*]

[a] *University of Pisa, Dipartimento di Chimica e Chimica Industriale, Via G. Moruzzi 13, I-56124 Pisa, Italy.*

[b] *Regional Centre of Advanced Technologies and Materials, Czech Advanced Technology and Research Institute, Palacký University, Šlechtitelů 27, CZ-779 00 Olomouc, Czech Republic.*

[c] *University of Pisa, Dipartimento di Farmacia, Via Bonanno Pisano 33, 56126 Pisa, Italy.*

[d] *University of Bologna, Dipartimento di Chimica Industriale "Toso Montanari", Viale del Risorgimento 4, I-40136 Bologna, Italy.*

[e] *Department of Cell Biology and Genetics, Faculty of Science, Palacký University, Šlechtitelů 27, CZ-779 00 Olomouc, Czech Republic*

Corresponding Authors.

[*]E-mail addresses: lorenzo.biancalana@unipi.it zdenek.travnicek@upol.cz valeria.dibussolo@unipi.it

Abstract

Glycoconjugation is a powerful tool to improve the anticancer activity of metal complexes. Herein, we modified commercial arylphosphanes with carbohydrate-derived fragments for the preparation of novel glycoconjugated ruthenium(II) *p*-cymene complexes. Specifically, D-galactal and D-allal-derived vinyl epoxides (**VEβ** and **VEα**) were coupled with (2-hydroxyphenyl)diphenylphosphane, affording the 2,3-unsaturated glycophosphanes **1β** and **1α**. Ligand exchange with $[Ru(C_2O_4)(\eta^6\text{-}p\text{-cymene})(H_2O)]$ gave the glycoconjugated complexes **Ru1β** and **Ru1α** which were subsequently dihydroxylated with OsO_4/*N*-methylmorpholine *N*-oxide to **Ru2β** and **Ru2α** containing *O*-benzyl D-mannose and D-gulose units respectively. Besides, aminoethyl tetra-*O*-acetyl-β-D-glucopyranoside was condensed with borane-protected (4-diphenylphosphanyl)benzoic acid by HATU/DIPEA under MW heating, to afford the amide **3·BH₃**. Zemplén deacylation with MeONa/MeOH gave the deprotected D-glucopyranoside derivative **4·BH₃**. The glycoconjugated phosphane complexes **Ru3** and **Ru4** were obtained by reaction of the phosphane-boranes **3·BH₃** and **4·BH₃** with $[Ru(C_2O_4)(\eta^6\text{-}p\text{-cymene})(H_2O)]$. The employed synthetic strategies were devised to circumvent unwanted phosphine oxidation. The compounds were purified by silica chromatography, isolated in high yield and purity and characterized by analytical and spectroscopic (IR and multinuclear NMR) techniques. The behaviour of the six glycoconjugated Ru complexes in aqueous solutions was assessed by NMR and MS measurements. All compounds were screened for their *in vitro* cytotoxicity against A2780/A2780R human ovarian and MCF7 breast cancer cell lines, revealing a significant cytotoxicity for complexes containing the 2,3-unsaturated glycosyl unit (**Ru1β, Ru1α**). Additional studies on five other human cancer cells, as well as time-dependent toxicity and cell-uptake analyses on ovarian cancer cells, confirmed the prominent activity of these two compounds – higher than cisplatin – and the better performance of the β anomer. However, **Ru1β, Ru1α** did not show preferential activity against cancer cells with respect to fetal lung fibroblast and human embryonic kidney cells as models of normal cells. The effects of the two ruthenium glycoconjugated compounds in A2780 ovarian cancer cells were further investigated by cell cycle

analysis, induction of apoptosis, intracellular ROS production, activation of caspases 3/7 and disruption of mitochondrial membrane potential. The latter is a relevant factor in the mechanism of action of the highly cytotoxic **Ru1β**, inducing cell death by apoptosis.

Keywords: anticancer metal complexes; phosphane ligand; ruthenium(II) arene; glycoconjugation; carbohydrate complexes; cytotoxicity; cell-cycle; apoptosis; mitochondrial membrane potential.

Introduction.

Different types of ruthenium complexes have been intensively investigated as possible alternatives to platinum-based anticancer drugs;[1] most notably Ru(III) derivatives NAMI-A ([ImH$_2$][*trans*-RuCl$_4$(κS-DMSO)(κN-Im)]; ImH = 1*H*-imidazole) and KP1019/NKP-1339 ([*trans*-RuCl$_4$(κN-Ind)$_2$]⁻, Na⁺ or IndH$_2$⁺ salt; IndH = 1*H*-indazole) underwent clinical trials.[2] In recent years, ruthenium(II) arene complexes rose to prominence in the pharmacological setting, showing a diversity of biological effects depending on the nature of the co-ligands.[3] The leading compound RAPTA-C ([RuCl$_2$(η^6-*p*-cymene)(PTA)]; Figure 1a), featuring 1,3,5-triaza-7-phosphaadamantane (PTA) as hydrophilic phosphane ligand, demonstrated considerable antimetastatic, antiangiogenic and antiinvasive properties, and is set to enter clinical trials.[4]

In this framework, tethering bioactive molecules represents an appealing strategy to increase the versatility and the selectivity of anticancer metal complexes.[5] Among these, carbohydrate ligands are excellent candidates, due to their biocompatibility and the possibility of modulating chemico-physical properties of the complex and minimizing its toxicity.[6] Furthermore, the carbohydrate unit is a pivotal organic structure for selective interactions with cancer cells.[7] Indeed, it is now widely known that carbohydrates play essential roles in intercellular and intracellular processes and also play key-roles in cancer diseases, characterized by a dysregulated glycosylation, where abnormal cell surface glycoconjugates contribute to tumour growth and metastasis.[8] In addition, tumour cells exhibit

dysfunctional metabolism, known as the Warburg effect, which consists in an augmented glucose avidity and high rates of aerobic glycolysis in order to sustain their high proliferation rate. As a consequence, transport membrane proteins such as glucose transporters (GLUTs) are overexpressed in cancer compared to normal tissues. Therefore, a promising strategy for targeting dysregulated metabolism is glycoconjugation, by linking a metal complex to glucose or to another sugar portion for the synthesis of potential metal-based anticancer drugs or cancer diagnostic agents.[6,9]

To date, a large number of metal-carbohydrate complexes have been tested on cancer cells and this strategy was successful in terms of enhanced biological activity in several cases.[10] On the other hand, glycoconjugation of ruthenium(II) arene complexes has been only limitedly explored thus far, also because of the synthetic effort in realizing such compounds. More specifically, some 3,5,6-bicyclophosphite-α-D-glucofuranoside derivatives[11] were employed as monodentate *P*-donor ligands to produce a family of $[RuX_2\{P(OR)_3\}(\eta^6\text{-arene})]$ and $[RuCl(PPh_3)\{P(OR)_3\}(\eta^6\text{-arene})]^+$ complexes, featuring various arenes and anionic co-ligands (Figure 1b).[12] In this respect, halide complexes revealed a complex speciation in aqueous medium[12a,d] and their replacement with bidentate 1,2-dicarboxylates (oxalate, malonate) resulted in superior stability.[12c] However, *in vitro* screening revealed an overall modest cytotoxicity, cellular uptake and cancer cell selectivity of these complexes.[12] Later, some elaborated 2,3-diaminopyranosides were coordinated to $Ru(\eta^6\text{-arene})$ scaffolds and exhibited moderate antiproliferative activity on some cancer cell lines (Figure 1c).[13] The first ruthenium(II) arene *half-sandwich* complexes comprising a fully deprotected hexose, *i.e.* glucose or galactose, and their *O*-acetylated or *O*-benzoylated derivatives, were only recently described (Figure 1d,e).[14,15] The key triazole ring in the monodentate *C*-/*N*- or bidentate *N,N*- ligands was constructed via glycosyl azides, and some of these complexes manifested considerable antiproliferative activity on cancer cells (A2780, ovarian) associated with low toxicity on normal cells (fibroblasts).[15] Interestingly, *sandwich* ruthenium(II) cyclopentadienyl complexes with a glucose-modified arene ligand were recently reported to be non-cytotoxic but very effective to impede cancer cell migration (Figure 1f).[16]

In the present work, we report the synthesis and characterization of new glycoconjugated ruthenium(II) *p*-cymene complexes and a study of their anticancer activity *in vitro*. Besides more notable monosaccharides (like glucose or mannose), our work also focused on 2,3-unsaturated hexoses, which are of particular appeal considering their use in medicinal chemistry.[17] Moreover, 2,3-unsaturated glycosides confer higher lipophilicity to the system, by comparison with their fully hydroxylated counterpart, with consequent increased activity against cancer cell lines.[18]

We decided to introduce the selected carbohydrate units via a phosphane ligand, providing a robust scaffold for the conjugation of bioactive molecules and other probes to anticancer metal complexes.[19] Specifically, we selected commercial (2-hydroxyphenyl)diphenylphosphane and (4-diphenylphosphanyl)benzoic acid as building blocks and we developed suitable synthetic strategies to exploit their hydroxyl and carboxylic acid functions to link the carbohydrate moiety.
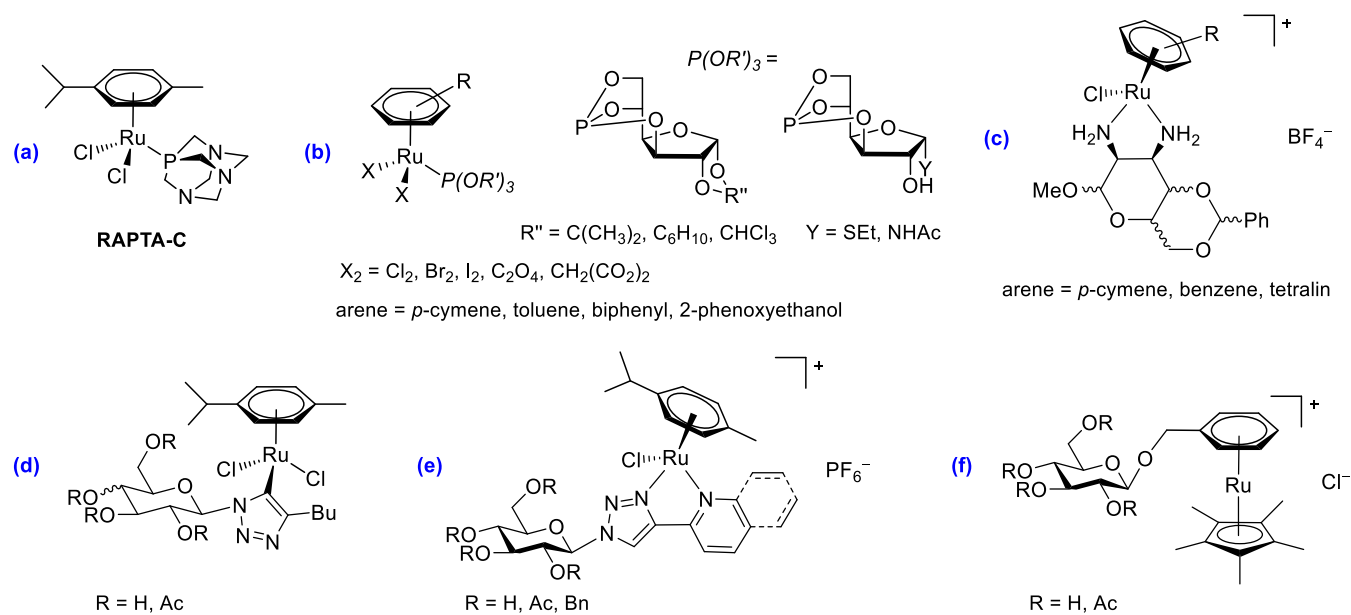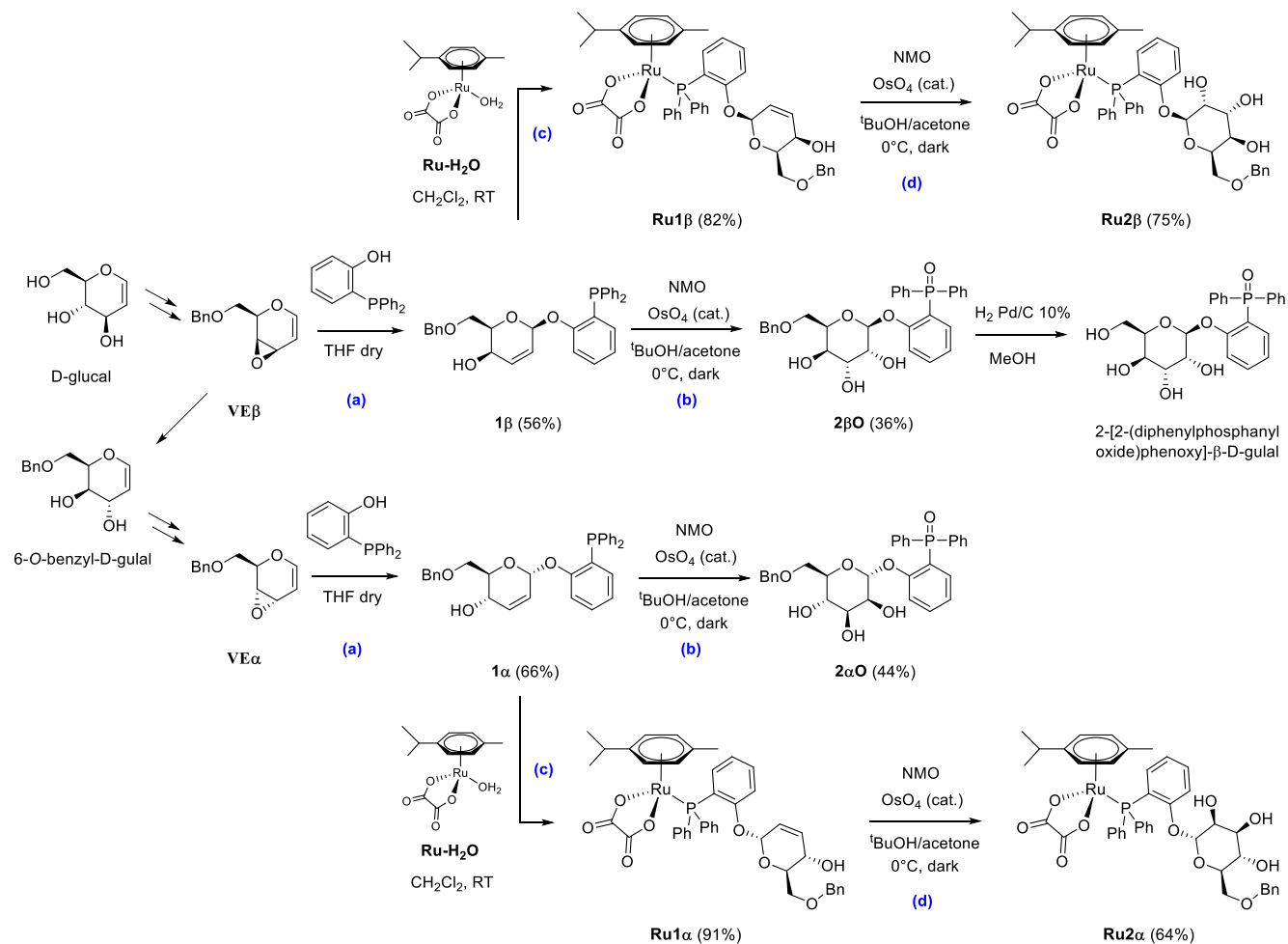

Figure 1. Structure of the anticancer complex RAPTA-C (**a**) and Ru(II)-η^6-arene complexes with various glycoconjugated ligands (published year in italics): 3,5,6-bicyclophosphite-α-D-glucofuranoside (*2008-2013*, **b**), 2,3-diamino-4,6-*O*-benzylidene-2,3-dideoxy-α-D-pyranosides of mannose, talose, gulose, glucose (*2015*, **c**), glucose- and galactose-modified 1,2,3-triazolylidene (*2019*; **d**), glucose-modified 2-pyridyl/quinolyl 1,2,3-triazole (*2021*, **e**), *sandwich* complexes with a glucose-derivatized arene (*2020*, **f**).

Results and discussion.

1. Synthesis and characterization of compounds.

Glycosylated phosphanes **1β** and **1α** were obtained following a completely regio- and stereoselective glycosylation process that we previously reported.[20] Glycosyl donors are represented by β- and α-vinyl epoxides **VEβ** and **VEα**, formally derived from D-galactal and D-allal.[21] These systems are characterized by a peculiar property: in the presence of nucleophiles such as alcohols, they undergo a completely 1,4-regio- and stereoselective conjugate addition affording 2,3-unsaturated glycosides with the same configuration as the starting epoxide (*i.e.* from α-epoxide is obtained α-2,3-unsaturated glycoside). Thus (2-hydroxyphenyl)diphenylphosphane was added to an *in situ* prepared solution of vinyl epoxide, obtained by treatment of the corresponding *trans*-hydroxy mesylate with *t*-BuOK.[22] The glyco-phosphanes **1β** and **1α** were purified by flash column chromatography and isolated in good yield (Scheme 1a). Subsequently, the double bond in **1β** and **1α** underwent dihydroxylation using OsO_4/*N*-methylmorpholine *N*-oxide (NMO), according to a previously-optimized protocol.[23] However, such conditions caused unwanted phosphorous oxidation, affording **2βO** and **2αO** (Scheme 1b). Hydrogenation of **2βO** with H_2 (1 bar) was effective for benzylether removal but did not reduce the phosphane oxide. Other protocols[24] for P=O reduction were tested ($LiAlH_4$/$CeCl_3$ in THF under reflux; $LiAlH_4$/$NaBH_4$/$CeCl_3$ in THF at 0 °C) but were not successful. Therefore, an alternative synthetic strategy was devised. First, compounds **Ru1β** and **Ru1α** were obtained by the straightforward reaction of $[Ru(C_2O_4)(p\text{-cymene})(H_2O)]$ (**Ru-H₂O**) with phosphanes **1β** and **1α** in dichloromethane (Scheme 1c). Next, OsO_4/NMO dihydroxylation of **Ru1β** and **Ru1α** afforded the desired complexes **Ru2β** and **Ru2α** (Scheme 1d). The latter reaction proceeded smoothly with **Ru2β** but was considerably slower with the α-stereoisomer, probably also because of solubility issues. To the best of our knowledge, these dihydroxylations are among the few that have been carried out on a *4d* or *5d* metal complex,[25] highlighting the inertness of the Ru(II)-arene scaffold and the coordinated phosphorous atom towards

6

such oxidizing conditions. Attempts to deprotect the benzyl ether group in **Ru2β** and **Ru2α** and by Pd-catalysed hydrogenation were unsuccessful.

Scheme 1. Preparation of glycosylated phosphanes **1β**, **1α** starting from vinyl epoxides **VEβ**, **VEα** and (2-hydroxyphenyl)diphenylphosphane (step **a**); subsequent reaction with [Ru(C₂O₄)(*p*-cymene)(H₂O)] to give **Ru1β**, **Ru1α** (step **c**). Upjohn dihydroxylations, affording benzyl-protected D-mannose and D-gulose conjugated phosphane oxides **2βO**, **2αO** (step **b**) and Ru complexes **Ru2β**, **Ru2α** (step **d**). NMO = *N*-methylmorpholine *N*-oxide. Isolated yields are given in parentheses.

Our next goal was to obtain a D-glucose-functionalized phosphane using (4-diphenylphosphanyl)benzoic acid as starting material and 2-aminoethanol as short alkyl linker providing an amide group to join the two fragments. In this regard, we noticed that only a small number of phosphanes containing a fully deprotected monosaccharide unit (glucose, galactose) have been

7

described in the literature.[26] The synthetic route we employed is based on a typical trichloroacetimidate-mediated glycosylation protocol.[27] Specifically, the trichloroacetimidate derivative, synthesized from commercial D-glucose,[28] was readily converted into 1-O-(2-azidoethyl)-2,3,4,6-tetra-O-acetyl-β-D-glucopyranoside by reaction with a freshly prepared solution of 2-azidoethanol.[29] Subsequent Pd-catalysed hydrogenation[30] of the terminal azido group gave the respective aminoethyl tetra-O-acetyl-β-D-glucopyranoside (Scheme 2a). Next, a HATU/DIPEA-mediated condensation of (4-diphenylphosphanyl borane)benzoic acid[31] with the amine was carried out in a microwave reactor, affording the glucophosphane borane **3·BH₃** (Scheme 2b). Finally, **3·BH₃** was fully deacetylated by treatment with a freshly prepared solution of MeONa in MeOH, in order to obtain 1-O-[2-(4-diphenylphosphanyl borane)benzamide]-β-D-glucopyranoside **4·BH₃** (Scheme 2c).[32] In this regard, the use of bench-stable phosphane-boranes was crucial to avoid irreversible oxidation at the phosphorous atom during workup.[26,29g,33] Indeed, analogous reactions carried out directly with 4-(diphenylphosphanyl)benzoic acid led to the isolation of the corresponding phosphane oxides **3O** and **4O** (see ESI). Finally, glycoconjugated complexes **Ru3** and **Ru4** were synthesized from [Ru(C₂O₄)(p-cymene)(H₂O)] and the respective phosphane-boranes **3·BH₃** and **4·BH₃** (Scheme 2d), following optimization of the reaction conditions with Ph₃PBH₃ (see ESI). It is worth noting that only few phosphane metal complexes have been prepared directly from the respective borane adducts;[34] more frequently, the BH₃ group is removed in a preliminary step or *in situ* by adding suitable amines.[35] A reference ruthenium compound devoid of the glucose moiety, **Ru5**, was prepared by EDCI/DMAP mediated coupling of 4-(diphenylphosphanyl)benzoic acid with 2-aminoethanol, followed by reaction of the phosphane **5** with [Ru(C₂O₄)(p-cymene)(H₂O)] (Scheme 2e and ESI).
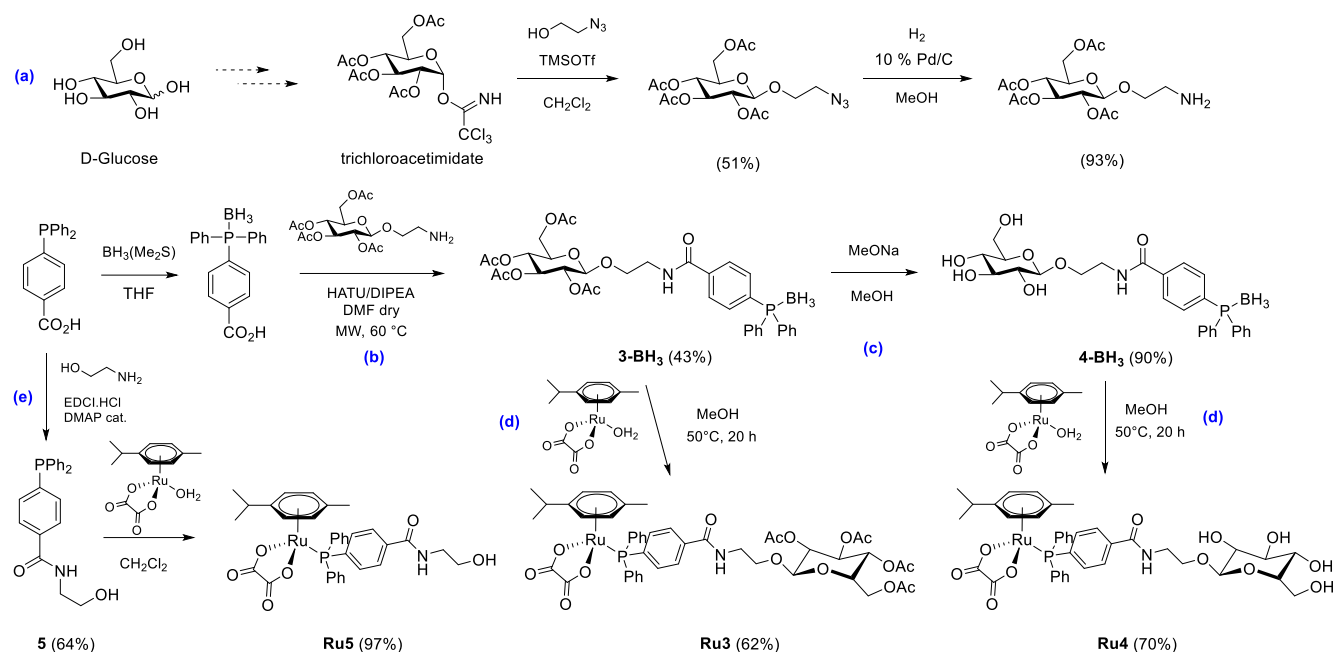
Scheme 2. Synthesis of glucose-modified phosphane-boranes **3-BH₃** and **4-BH₃** starting from D-glucose, 2-azidoethanol and (4-diphenylphosphanyl)benzoic acid: preparation of the tetra-acetylated glucose with pendant amine group (path **a**), amide coupling (step **b**) and deacetylation (step **c**); preparation of the corresponding ruthenium(II) *p*-cymene complexes **Ru3**, **Ru4** with B to Ru transfer of the phosphane unit (step **d**); preparation of the reference complex **Ru5** devoid of the sugar fragment (path **e**). TMSOTf = trimethylsilyl triflate: EDCI = 1-ethyl-3-(3-dimethylaminopropyl)carbodiimide; DMAP = 4-dimethylaminopyridine. Isolated yields are given in parentheses.

Ruthenium complexes **Ru1-4** were purified by silica gel chromatography and isolated in 64−91 % yield as air-stable yellow solids. The glycophosphanes and their derivatives (**1β**, **1α**, **2βO**, **2αO**, **3·BH₃**, **4·BH₃**) as well as ruthenium complexes **Ru1**-**Ru5** are unprecedented and were characterized by analytical (CNH analyses, optical rotation) and spectroscopic (solid state attenuated total reflection IR, $^1H/^{13}C/^{31}P$ and 2D NMR in organic solvents) techniques. IR and NMR spectra are supplied in Figures S1-S53; selected ^1H NMR data related to the pyranoside ring is given in Table 1. In addition, the crystal structure of the ruthenium precursor [Ru(C₂O₄)(*p*-cymene)(H₂O)] (**Ru-H₂O**) was ascertained by an X-ray diffraction study (see Figure S54 and Tables S2-S3).

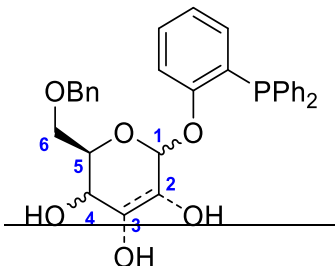In ^{31}P NMR spectra, ruthenium complexes display a sharp singlet in the 25-27 (**Ru1β**, **Ru1α**) or 31-34 (**Ru2-Ru5**) ppm range, to be compared with – 15 ppm for the glycoconjugated phosphanes (**1β**, **1α**),

31-33 ppm for the phosphane oxides (**2βO**, **2αO**, **3O**, **4O**) and 21 ppm for the phosphane-boranes (**3·BH₃**, **4·BH₃**). The phosphorous resonances undergoes an appreciable downfield shift (*ca.* + 11 ppm) due to the change in coordination from boron (**3-4·BH₃**) to ruthenium (**Ru3-4**), useful for reaction monitoring.[36]

The anomeric proton was detected as a singlet ranging from 5.08 to 5.74 ppm in ^{1}H NMR spectra of **Ru1α/β** and **Ru2α/β** (Table 1), whereas it appeared as doublet around 4.30-4.70 ppm for glucose-functionalized **Ru3** and **Ru4**. The ^{1}H and ^{13}C NMR resonances of CH groups of the *p*-cymene ring, of the two isopropyl CH₃ groups and of the oxalate ligand in **Ru1α/β** and **Ru2α/β** are anisochronous, due to spatial proximity (and reduced overall symmetry) of the chiral glycosyl moiety on the phosphane ligand;[37] in particular, the two isopropyl groups are diastereotopic and their presence represents the source of inequivalence for the arene resonances, which is magnetic in origin (by coupling criterion). This effect seemed to be less appreciable in **Ru3** and **Ru4**, likely because of the increased distance (lower chiral perturbation) between the metal centre and the sugar moiety. For comparison, ^{1}H NMR spectra of C_s-symmetric **Ru-H₂O** and **Ru5** show two doublets for the η^6-arene protons.

The dihydroxylation of the double bond of **1β**, **1α** and their Ru complexes is accompanied by a marked shielding of the related ^{1}H and ^{13}C NMR resonances, the latter moving from *ca.* 130 (C=C) to 70 (C-O) ppm. Notably, all ^{1}H NMR signals of the pyranoside ring and the aromatic protons of the *p*-cymene ligand are considerably downfield-shifted in **Ru2β** with respect to **Ru2α** (Table 1).

Table 1. Comparison of selected ^{1}H and ^{13}C NMR (in *italics*) chemical shifts for the pyranoside ring in **1β**, **1α**, **2βO**, **2αO** and related Ru(II) *p*-cymene complexes.[a]

Compound	Pyranoside CHₓ NMR δ / ppm						C atom numbering
	1	2	3	4	5	6	
1β	5.51	6.04	5.31	3.81	3.70	3.95	
	97.6	*128.5*	*134.1*	*73.6*	*74.6*	*62.8*	
Ru1β	5.45	4.69	5.91	3.90–3.83		3.64	
	95.5	*128.1*	*131.3*	*62.2*	*74.9*	*69.8*	
1α	5.48 *93.4*	5.28	5.88 *133.7*	4.19 *70.8*	3.77	3.6	

10

		128.4			*73.7*	*65.3*
Ru1α	5.38	4.45	5.65	3.86	3.10	3.65, 3.53
	94.4	*124.6*	*136.1*	*63.8*	*74.0*	*70.6*
2βO	5.06	4.21	3.93	3.77	4.12	3.83
	96.5	*73.5*	*74.6*	*69.9*	*76.3*	*62.9*
Ru2β	5.74	4.25	4.06	3.86	4.42	3.81–3.71
	98.0	*67.9*	*73.6*	*71.2*	*74.0*	*71.1*
2αO	5.31		3.77-3.76			3.51, 3.10
	93.4	*72.3*	*73.7*	*70.3*	*75.7*	*65.2*
Ru2α	5.08	2.57	2.44	3.35	3.13	3.69, 3.57
	101.1	*70.6*	*71.5*	*68.0*	*74.7*	*71.1*

[a] NMR data (without multiplicity) in CDCl$_3$ for **1β**, **1α**, **2βO**, **2αO** and **Ru1β** (^{13}C); in CD$_3$OD for **Ru1α**, **Ru2β**, **Ru2α** and **2αO** (^{1}H).

2. Behaviour of Ru complexes in aqueous media

With a view to the biological application, the behaviour of the ruthenium complexes in aqueous solution was studied by NMR. Therefore, solutions of **Ru1-5** in D$_2$O or D$_2$O/DMSO-d$_6$ mixtures[38] (*ca.* 5 mM) were maintained at 37 °C and monitored by ^{1}H and ^{31}P NMR (see Experimental). Under these conditions, **Ru2β**, **Ru2α**, **Ru3** and **Ru4** displayed an excellent inertness, with > 90% of starting material detected in solution after 72 h (Table S4). On the contrary, **Ru1β** and **Ru1α** underwent pronounced changes, even after comparatively shorter times (20 h). A common product formed in the solutions of **Ru1α/β** and **Ru2α/β** is [Ru(C$_2$O$_4$H){Ph$_2$P(2-C$_6$H$_4$O)}(η^6-*p*-cymene)], **Ru6**, resulting from hydrolysis of the glycosidic linkage (Scheme S2), as confirmed by independent synthesis of the compound from [Ru(C$_2$O$_4$)(*p*-cymene)(H$_2$O)] and (2-hydroxyphenyl)diphenylphosphane (see ESI and ref.[39]). The much higher reactivity of **Ru1α/β** with respect to their hydroxylated derivatives **Ru2α/β**, under equal conditions, could be related to reactivity of the double bond on the pyranose ring or its allylic position (*i.e.* the anomeric carbon).

Similar experiments with **Ru2β**, **Ru2α**, **Ru3**-**Ru5** were then performed in the presence of cell culture medium (RPMI-1640) at 37 °C for 72 h (5 % DMSO). Compounds **Ru2β** and **Ru2α** once again demonstrated a remarkable inertness, as indicated by the ^{1}H NMR spectra of the residues obtained from

11

CH$_2$Cl$_2$ extraction of the final solution (Figures S55-S56). Instead, progressive formation of phosphane oxides over time was observed in the solutions of **Ru3**-**Ru5**. Complex **Ru3** also underwent deacetylation processes, as ascertained by ESI-MS (Figure S57). Thus, from a biological perspective, complex **Ru3** can be viewed as a bioprecursor of **Ru4**, featuring a deprotected glucose unit.

The behaviour of the more reactive complexes **Ru1β** and **Ru1α** at micromolar concentrations was assessed by using electrospray-ionization (ESI) mass spectrometry. Thus, 10 μM solutions of **Ru1β** and **Ru1α** in a water/MeOH mixture (1:1) were analyzed by ESI-MS; mass spectra are shown in Figures S58–S62. The spectra measured immediately after dissolution revealed signals at $m/z = 843.22$ corresponding to the respective pseudomolecular ion [**Ru1α/β**+Na]$^+$ and at $m/z = 535.25$ corresponding to the oxidized ligand [**1α/βO**+Na]$^+$. Another signal at $m/z = 513.15$ formally corresponds to a {Ru(p-cymene)}$^{2+}$ unit bound to a 2-(diphenylphosphanyl)phenolate ligand. This fragment is likely generated by loss of oxalate from **Ru6**, the compound that was NMR-detected in DMSO/water solutions of **Ru1β** and **Ru1α** (see above). The MS spectra of both **Ru1β** and **Ru1α** measured after 24 h at room temperature include new less intense signals in the 1009-1061 m/z range that can be attributed to the formation of various dimeric products; for a detailed evaluation of possible compositions of pseudomolecular ions, see Figures S59 and S61. It is interesting to note that dimeric products were also MS-detected by studying the hydrolytic process of related [RuCl$_2$(3,5,6-bicyclophosphite-α-D-glucofuranoside)(η^6-p-cymene)] complexes.[12a] Furthermore, solutions of **Ru1β** and **Ru1α** (10 μM in MeOH/water 1:1) were incubated with L-cysteine (L-Cys) or reduced glutathione (GSH) at normal physiological levels (290 and 6 μM, respectively) and monitored by ESI-MS (Figures S63-S68) over 24 h. Very small differences in MS spectra can be noticed with respect to the previous experiments, indicating no preferential and kinetically relevant interactions of the ruthenium complexes with the sulphur-containing biomolecules employed.

3. Biological studies

3.1. *In vitro* cytotoxicity on cancer and normal cells

The cytotoxicity of all glycoconjugated ruthenium(II) arene complexes (**Ru1-4**) was firstly assessed on ovarian (A2780 and cisplatin-resistant A2780R) and breast (MCF7) cancer cell lines after 24 h incubation, together with selected compounds for comparative purposes (Table 2). MTT viability assay revealed that **Ru1β** and **Ru1α**, containing a 2,3-unsaturated glycosyl unit, are more cytotoxic than the benchmark anti-cancer drug cisplatin, especially on the cisplatin-resistant (A2780R) strain. The other ruthenium phosphane complexes, with (**Ru2-4**) or without (**Ru5**) carbohydrate functionalization and the corresponding glycophosphane oxides (**2βO**, **2αO**, **3O**, **4O**; except for **2βO** on A2780 cells), displayed a negligible cytotoxicity ($IC_{50} > 50$ µM in all cell lines). The substitutionally-labile complexes **Ru-H₂O**, [RuCl$_2$(η^6-*p*-cymene)]$_2$ and RAPTA-C did not affect the viability of A2780 cancer cells in the investigated concentration range, in alignment with their poor activity on various normal and cancerous cell lines as described elsewhere.[4a,40]

Table 2. Cell viability – MTT test of glycoconjugated ruthenium complexes, glycosylated phosphane oxides, RAPTA-C, [RuCl$_2$(η^6-*p*-cymene)]$_2$, [Ru(C$_2$O$_4$)(η^6-*p*-cymene)(H$_2$O)] (**Ru-H₂O**) and cisplatin on human ovarian (A2780, A2780R) and breast (MCF7) cancer cells. Cells were incubated with tested compounds for 24 h; results are expressed as mean IC_{50} values with standard deviations (SD) calculated from three consecutive cell passages.

Compound	IC_{50} (24 h) / µM		
	A2780	A2780R	MCF7
Ru1β	3.7 ± 1.1	2.3 ± 0.4	7.8 ± 0.3
Ru1α	11.5 ± 1.6	10.0 ± 1.3	19.5 ± 3.1
Ru2β	> 50	> 50	> 50
Ru2α	> 50	> 50	> 50
Ru3	> 50	> 50	> 50
Ru4	> 50	> 50	> 50
Ru5	> 50	> 50	> 50
2βO	45.4 ± 3.7	> 50	> 50
2αO	> 50	> 50	> 50
3O	> 50	> 50	> 50
4O	> 50	> 50	> 50
[RuCl$_2$(η^6-*p*-cymene)]$_2$	> 50	-	> 100 [a]

13

Ru-H₂O	> 50	-	-
RAPTA-C	> 50	> 50	> 50
cisplatin	14.9 ± 1.0	37.7 ± 0.8	20.9 ± 2.8

[a] After 48 h incubation, taken from the literature.[40b]

Next, we tested the *in vitro* cytotoxicity of the most active Ru(II) complexes **Ru1β**, **Ru1α** and cisplatin in human liver (HepG2) osteosarcoma (HOS) prostate (PC-3), lung (A549) and cervical (HeLa) cancer cells. Fetal lung fibroblast (MRC-5) and human embryonic kidney cells (HEK-293) were included as healthy cells. IC_{50} data are compiled in Table 3, whilst dose-response curves of complexes **Ru1β** and **Ru1α** regarding all the cell lines used are given in Figure S69. Both **Ru1β** and **Ru1α** displayed a cytotoxicity higher than cisplatin in all the tested cancer cell lines, besides, **Ru1β** is always more cytotoxic than its stereoisomer **Ru1α** (average IC_{50} 5.6 and 16 µM, respectively). However, it should be noted that the toxicity of **Ru1β** and **Ru1α** on normal cells (MRC-5 and HEK-293) is comparable to that observed in cancer cells, implying no preferential activity against the latter.

Table 3. Cell viability – MTT test of **Ru1β**, **Ru1α** and cisplatin on human liver (HepG2) osteosarcoma (HOS) prostate (PC-3), lung (A549), cervical (HeLa) cancer cells, fetal lung fibroblast (MRC-5) embryonic kidney cells (HEK-293). Cells were incubated with tested compounds for 24 h; results are expressed as mean IC_{50} values with standard deviations (SD) calculated from three consecutive cell passages.

Compound	IC_{50} (24 h) / µM						
	HepG2	HOS	PC-3	A549	HeLa	MRC-5	HEK-293
Ru1β	5.2 ± 0.6	6.4 ± 0.4	6.0 ± 0.5	7.7 ± 0.4	5.6 ± 0.2	3.7 ± 0.6	3.8 ± 0.6
Ru1α	18.3 ± 1.3	15.7 ± 1.8	16.8 ± 0.5	23.3 ± 0.8	13.2 ± 0.4	12.9 ± 0.7	12.8 ± 1.0
cisplatin	20.8 ± 1.7	32.0 ± 5.9	> 50	38.4 ± 1.6	17.1 ± 0.7	> 80	> 80

Subsequently, time-dependent effects (24, 48 and 72 h) of **Ru1β**, **Ru1α** and cisplatin on the viability of cancer (A2780) and normal (MRC-5 and HEK-293) cells were evaluated (Table 4). The cytotoxicity of cisplatin significantly increased with incubation time in all the cell lines tested; this behaviour is well documented in the literature.[41] Similarly, **Ru1α** showed a moderate decrease in IC_{50} values between 24 and 48 h incubation and very small changes in the following 24 h. On the other hand, the cytotoxicity

14

of **Ru1β** remained nearly constant in the studied time range (24 – 72 h). Notably, both Ru complexes are more toxic than cisplatin at each incubation time, but they lack a substantial cancer cell selectivity also after 24 and 48 h treatment.

Table 4. Cell viability – MTT test on A2780, MRC-5 and HEK-293 cells incubated with **Ru1β**, **Ru1α** or cisplatin for 24, 48 and 72 h. Results are expressed as mean IC_{50} values with standard deviations (SD) calculated from three consecutive cell passages.

Compound	IC_{50} / μM, A2780			IC_{50} / μM, MRC-5			IC_{50} / μM, HEK-293		
	24 h	48 h	72 h	24 h	48 h	72 h	24 h	48 h	72 h
Ru1β	5.6 ± 1.1	3.1 ± 0.5	3.6 ± 0.9	3.7 ± 0.6	3.0 ± 0.1	3.2 ± 0.5	3.8 ± 0.6	2.9 ± 0.7	2.7 ± 0.2
Ru1α	12.2 ± 1.7	4.0 ± 0.6	3.0 ± 0.1	12.9 ± 0.7	7.6 ± 1.6	8.2 ± 1.8	12.8 ± 1.0	4.4 ± 0.9	3.7 ± 0.4
cisplatin	20.6 ± 2.9	11.6 ± 0.5	7.6 ± 2.7	> 80	19.9 ± 4.6	11.7 ± 2.2	> 80	19.6 ± 4.8	8.5 ± 3.1

3.2. Cellular uptake on A2780 cells

The A2780 cells were treated by equitoxic IC_{50} concentrations (for 24 h incubation time) of **Ru1β** or **Ru1α**, washed and isolated after different incubation times (2, 6, 12, 24 and 48 h) and ruthenium content in the cells was determined by ICP-MS. Similar experiments were performed with cisplatin for comparative purposes and the platinum content was determined by the same method in the same batch of samples. The results, representing the dynamics of cellular uptake of the complexes into the A2780 cells, are displayed in Figure 2. The intracellular metal accumulation for cisplatin reached the maximum after 24 h and consequently decreased to 7.5 ng/10^6 cells after 48 h of incubation, a value comparable to that obtained after 2 h incubation. The downward trend can be related to "pre-target" inactivation, *e.g.* the inactivation with GSH or metallothioneins, and/or to exclusion processes,[42] *e.g.* by plasma membrane copper transporters or membrane ATP-dependent drug efflux proteins. Conversely, the ruthenium content in A2780 cells increased with the incubation time for both **Ru1β** and **Ru1α**. The dynamics of the concentration increase is almost linear with **Ru1α** while is it much more pronounced for **Ru1β**. Specifically, the ruthenium cellular levels are higher for **Ru1β** than for **Ru1α** at each time (*e.g.* 43 and 13 ng/10^6 cells after 24 h, respectively), but **Ru1α** was applied in *ca*. 3-times higher

15

concentration than **Ru1β**, according to their IC_{50}. Consequently, the cellular uptake of **Ru1β** proceeds much more effectively than for its stereoisomer **Ru1α**, and this result aligns with the time-dependent cytotoxicity discussed above.
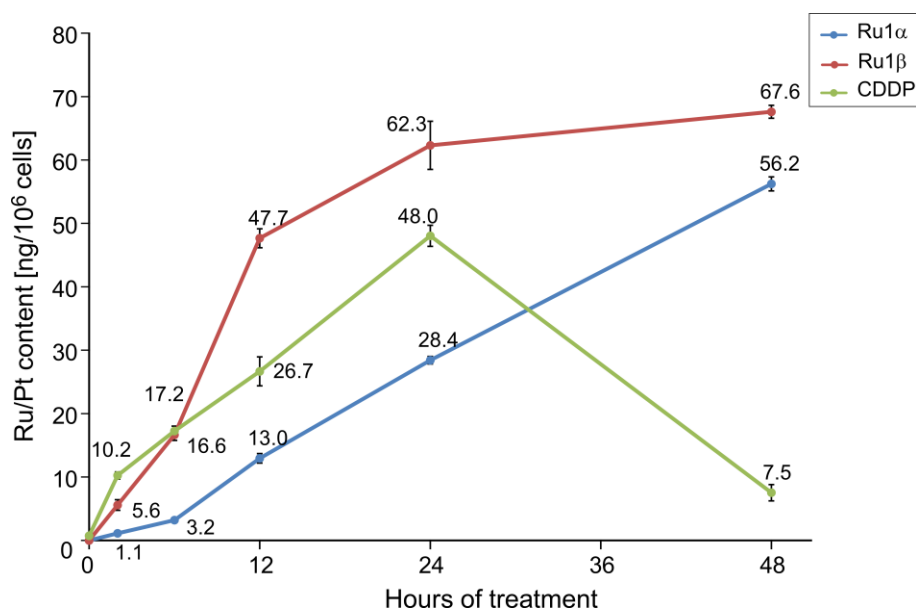
Figure 2. Time-dependent metal content profiles of **Ru1β** (red points), **Ru1α** (green points) and cisplatin (blue points) in A2780 cells as determined by ICP-MS (ng metal/10^6 cells) at various incubation times (0-48 h). The lines represent just a guide for eyes for better clarity of trends; the numbers represent the average values for the selected time period.

3.3. Cell cycle modification and induction of cell death on A2780 cells

Additional experiments were carried out on A2780 ovarian cancer cells in order to reveal cellular effects of the cytotoxic ruthenium complexes under investigation (**Ru1β** and **Ru1α**) and to gain insights on their mechanism of action.

First, the ability of **Ru1β**, **Ru1α** and cisplatin (as a reference compound) to modify the cell cycle was studied. Compounds were incubated at 15 μM for 24 h; a concentration at which both Ru complexes exert a considerable cytotoxicity (see Table 4). Results, shown in Figure 3, reveal a different accumulation of cells in the G0/G1, S and G2/M phases of the cell cycle for the ruthenium complexes as compared to cisplatin, which is known to arrest cancer cells in S-phase of the cell cycle.[43] Moreover,

16

the cell cycle profiles of **Ru1β** and **Ru1α** differ significantly from each other: **Ru1α** caused only marginal differences in comparison to the untreated control, whereas samples treated with **Ru1β** had significantly more cells accumulated in G2/M and S phase, with consequent lowering the portion of G0/G1 cells with respect to control. These findings indicate that the mechanism of action of **Ru1α** and **Ru1β** is completely different with respect to cisplatin and also between each other.
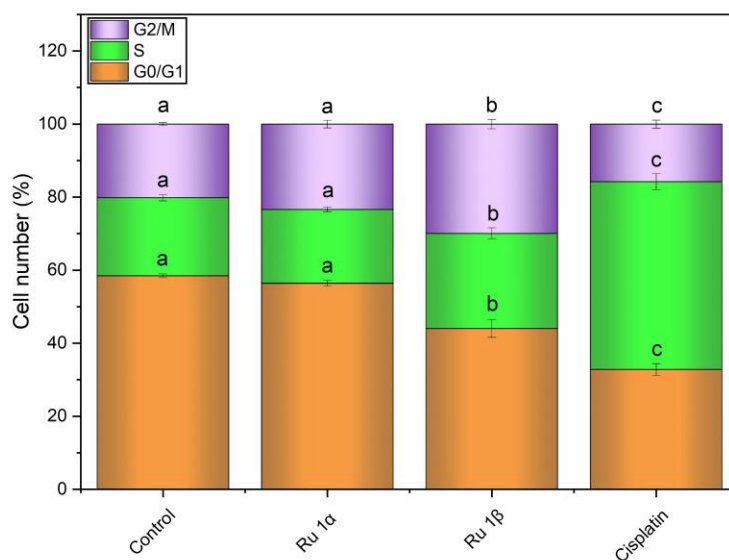
Figure 3. Effect of **Ru1β**, **Ru1α** and cisplatin on the cell cycle of the A2780 cancer cells after 24 h incubation, showing the significant effect of the **Ru1β** complex on lowering the portion of cells in the G0/G1 cell phase, while the number of cells in the G2/M cell phase increased significantly. Different small letters (a, b, c) indicate statistically significant differences at p ≤ 0.05.

Next, the induction of cell death was studied by means of the Annexin V/propidium iodide (PI) method using flow cytometry, under the same conditions as above (15 μM compounds, A2780 cells, 24 h incubation). Results are displayed in Figure 4; Annexin V - / PI - group represents surviving cells, Annexin V + / PI - group represents cells with disturbed membranes entering the early apoptosis, and Annexin V + / PI + group represents the cells in late stages of apoptosis with permeable cell and nuclear membranes. Treatment of the A2780 cells with **Ru1α** gave very similar results as untreated control. By contrast, **Ru1β** caused a significant increase in both Annexin V +/ PI – and Annexin V +/

PI + cells, thus it effectively induced the apoptosis and necrosis in the A2780 cells. The samples treated with cisplatin manifested increase of Annexin V +/ PI – and Annexin V +/ PI + cells, indicating apoptosis and necrosis progression in the A2780 cells, but less pronounced when compared to **Ru1β**. These findings, jointly with the cell cycle analysis and the previously discussed data, remark the different profiles of biological activity between **Ru1β**, **Ru1α** and cisplatin.
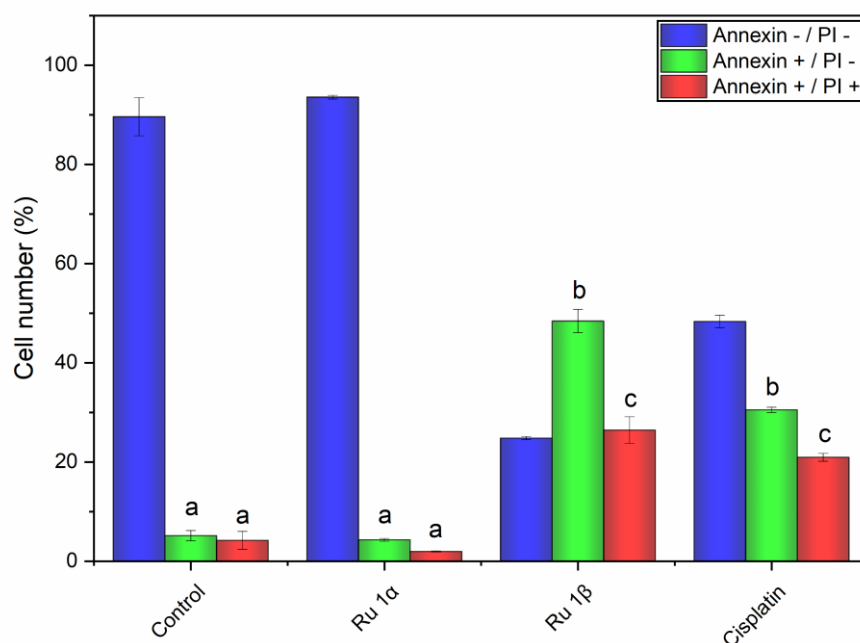

Figure 4. Effect of **Ru1β**, **Ru1α** and cisplatin on induction of different types of cell death in the A2780 cells after 24 h incubation, established by the flow cytometric analysis using the Annexin V and propidium iodide staining. Different small letters (a, b, c) indicate statistically significant differences at p ≤ 0.05.

3.4. Caspases 3/7 activation, mitochondrial membrane potential (MMP) and intracellular production of reactive oxygen species (ROS) on A2780 cells.

In order to outline possible mechanism of action of the complexes leading to cell death, we evaluated the ability of **Ru1β**, **Ru1α** and cisplatin as reference compound, to activate the executioner caspases 3/7 (Figure 5a) and to disrupt the mitochondrial membrane potential (MMP – Figure 5b). The

activation of executioner caspases 3/7 is connected with the destruction of intracellular cytoskeleton and other structural proteins of the cell in the process of apoptosis.[44] Treatment with **Ru1β** and cisplatin caused significant activation of caspases 3/7, while **Ru1α** had negligible effect. For the MMP analysis, **Ru1β** produced a significantly higher effect then the rest of the samples, with over 80 % of cells having damaged mitochondrial membrane. By contrast, cisplatin showed significant but lower disruption of MMP (44 % of cells had damaged mitochondria) and **Ru1α** caused only a slight increase in MMP disruption, not significant when compared to control cells. Therefore, the depolarization of mitochondrial membranes appears to be a dominant factor in the mechanism of action of **Ru1β**, which is possibly responsible for its significant cytotoxicity against cancer cells, as compared to the far less effective **Ru1α**.
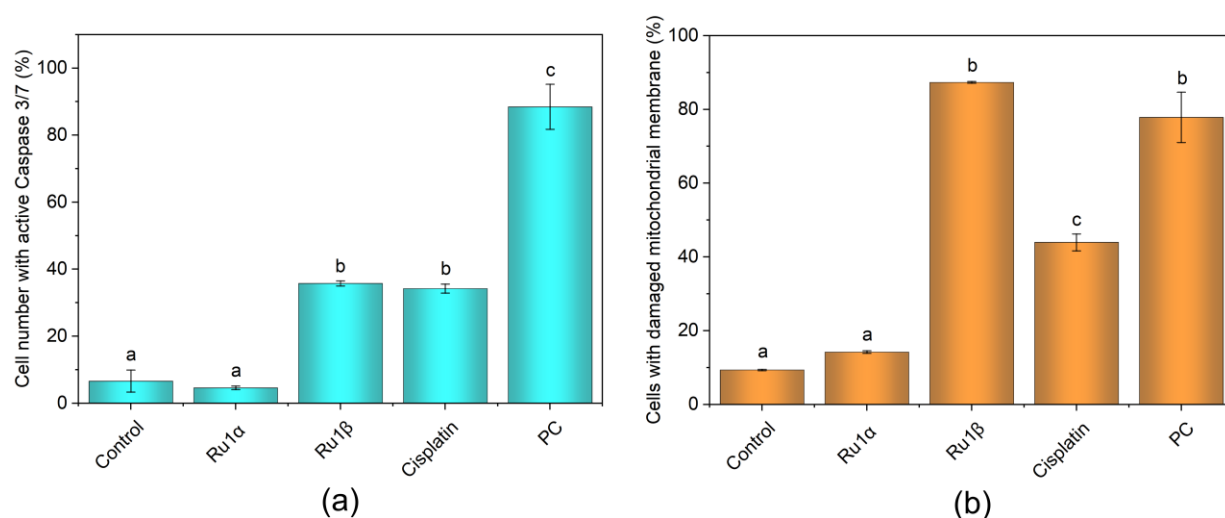
Figure 5. Effects of **Ru1β**, **Ru1α** and cisplatin on activation of the executioner caspases 3/7 **(a)** and on disruption of mitochondrial membrane potential **(b)** in the A2780 cells after 24 h incubation. Different small letters (a, b, c) indicate statistically significant differences at p ≤ 0.05.

Lastly we assessed the effects of the complexes on the overexpression of intracellular reactive oxygen species (ROS) and also, specifically, on the intracellular production of superoxide by means of a fluorometric method. In this respect, A2780 cells were incubated with **Ru1β**, **Ru1α** and cisplatin for 24 h and the oxidative stress was induced by addition of the known prooxidative agent pyocyanin (PC).[45]

Results indicate that both Ru complexes slightly decreased the formation of oxidative stress in A2780 cells (Figure S70). Such behaviour (*antioxidant* activity) was previously reported for other ruthenium(II) arene complexes, such as [RuCl(*p*-cymene)(L$_N$)]BF$_4$ compounds involving aromatic diimine ligands (L$_N$)[46] and complexes of the [RuCl(*p*-cymene)(L$_{NS}$)] type containing the 3-methoxysalicylaldehyde-4(N)-substituted thiosemicarbazones (L$_{NS}$).[47] On the other hand, Ru(II) polypyridyl complexes, with general formula [Ru(L$_N$)$_2$(HMHPIP)](ClO$_4$)$_2$, where L$_N$ represents aromatic diimine ligands and HMHPIP denotes {[2-(2-hydroxyl-3-methyl-5-hydroxylmethyl)-4-pyridyl]imidazo[4,5-f][1,10]-phenanthroline}[48] and ruthenium(II) *p*-cymene complexes containing benzimidazole-based ligands[49] showed, besides good antiproliferative effects, also the ability to promote the progression of oxidative stress in the cancer cells and thus induction of the cell death.

Conclusions.

In this work, we prepared a rare series of glycoconjugated ruthenium(II) *p*-cymene complexes and investigated their biological effects on cancer cells. For this purpose, we derivatized two commercially-available triarylphosphanes with various glycosyl units and six novel glycoconjugated Ru(II) *p*-cymene complexes were isolated in high yield and purity. The synthetic routes take advantage of highly regio- and stereoselective steps to modify the carbohydrate fragment and allow easier manipulation of the products by preventing undesired phosphorous oxidation. Compounds **Ru2β** and **Ru2α**, functionalized with a D-gulose and D-mannose group, respectively, as well as D-glucose-derivatized complexes **Ru3** and **Ru4** revealed a remarkable inertness in aqueous and/or cell culture medium solution at 37 °C, nevertheless they resulted non-cytotoxic in ovarian and breast cancer cell lines. Conversely, complexes containing 2,3-unsaturated glycosides (**Ru1β** and **Ru1α**) showed cytotoxic effects on eight different cancer cell lines, superior to those exerted by the anticancer drug cisplatin. In particular, **Ru1β** prevailed over its anomer **Ru1α** in all cytotoxicity tests. The time-resolved toxicity and metal content in A2780 cells reflect the rapid and effective cellular uptake of **Ru1β**. The peculiar mechanism of

action of **Ru1β**, distinct from that of **Ru1α** and cisplatin, involves disruption of mitochondrial membrane potential and consequently the activation of executioner caspases 3/7, resulting in a significant increase of early and late apoptotic cells. These findings corroborates the importance of this class of complexes as antiproliferative agents and pave the way to design more effective compounds. In this respect, increasing the cancer cell selectivity represents the primary goal. Besides, the two glycoconjugation methodologies developed in this work may be extended to other transition metal scaffolds investigated for anticancer activity.

Experimental.

1. General experimental details.

1-[Bis(dimethylamino)methylene]-1H-1,2,3-triazolo[4,5-b]pyridinium 3-oxide hexafluorophosphate (HATU), diisopropylethylamine, $Me_2S \cdot BH_3$, (2-diphenylphosphanyl)phenol, 4-(diphenylphosphanyl)benzoic acid and ethyl(diisopropylamino)carboxydiimide hydrochloride (EDCI·HCl) were purchased from Merck and stored under N_2. Anhydrous dimethylformamide (DMF), methanol, toluene, triethylamine (TEA) were used as received (Merck; "sure-seal" cap bottles); THF was distilled over Na/benzophenone, CH_2Cl_2 was distilled over P_2O_5. Other reactants and solvents were purchased from Alfa Aesar, Sigma Aldrich or TCI Europe. [$RuCl_2(\eta^6$-p-cymene)]$_2$ was prepared as described in the literature.[50] The synthesis of **1β**, **1α**, **3·BH₃**, **4·BH₃** and 4-(diphenylphosphanyl borane)benzoic acid was performed in flame-dried modified Schlenk (Kjeldahl shape) flasks fitted with a glass stopped or rubber septa under argon. Air and moisture-sensitive liquids and solutions were transferred via syringe. The synthesis of **3·BH₃** was performed in a microwave reactor Biotage® Initiator 4.1.4. Reactions were followed by thin-layer chromatography (TLC), performed on Merck silica gel (60 F_{254}) sheets that were visualized under a UV lamp (254 nm) and detected by 0.5% phosphomolybdic acid solution in 95% EtOH or 10% H_2SO_4 solution in 90% EtOH. Purification on silica gel columns were performed by flash (Kieselgel 40, 0.040–0.063 mm; Merck) or regular (Merck,

70-230 mesh) chromatography, as indicated. Organic solutions were dried on Na_2SO_4 or $MgSO_4$ and concentrated *in vacuo* by a rotary evaporator below 40°C. The synthesis of **Ru1β**, **Ru1α**, **Ru3-Ru6**, and $[Ru(C_2O_4)(\eta^6\text{-}p\text{-cymene})(PPh_3)]$ was performed under N_2 using standard Schlenk techniques. All the other operations were carried out in air with common laboratory glassware. Except where otherwise noted, compounds are air- and moisture-stable in the solid state for short time periods; they were maintained under N_2 at 4°C for long-term storage as a precaution. NMR spectra were recorded at 25 °C on Bruker Avance II DRX400 or Bruker UltraShield 400 spectrometers. Chemical shifts (ppm) are referenced to the residual solvent peaks[51] (^1H, ^{13}C) or to external standards[52] (^{11}B to 15% $BF_3 \cdot OEt_2$ in $CDCl_3$, ^{31}P to 85% H_3PO_4). ^1H and ^{13}C spectral assignments were aided by $^1H\{^{31}P\}$, ^{13}C DEPT 135, ^1H-^1H COSY, ^1H-^{13}C *gs*-HSQC and ^1H-^{13}C *gs*-HMBC and NOESY experiments. $CDCl_3$ stored in the dark over Na_2CO_3 was used for NMR analysis. IR spectra (650-4000 cm^{-1}) of pure samples were recorded on Perkin Elmer Spectrum One or Agilent Cary 600 FT-IR spectrometers, equipped with Attenuated Total Reflectance (ATR) sampling accessory. Optical rotations were measured with a ATAGO AP-300 Automatic Polarimeter at 20 °C. Carbon, hydrogen and nitrogen analyses were performed on a Vario MICRO cube instrument (Elementar).

2. Synthesis of glycosylated triarylphosphanes.

(1*R*,4*R*,5*R*)-5-(Benzyloxymethyl)-4-hydroxy-1-[2-(diphenylphosphanyl)phenoxy]-2H-2,3-dihydropyran, 1β (Chart 1).

**Chart 1**. Structure of **1β** (refer to Chart S10 for C atom numbering).
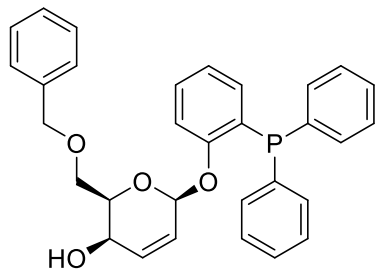
A solution of 4-*O*-mesyl-6-*O*-(benzyl)-D-glucal prepared as reported in literature,[53] (136.4 mg, 0.444 mmol) in anhydrous THF (3.11 mL) was treated with *t*-BuOK (64 mg, 0.57 mmol) at room temperature in a Schlenk flask. After stirring for 30 minutes at the same temperature, the time necessary for the cyclization of 4-*O*-mesyl-6-*O*-(benzyl)-D-glucal to the corresponding vinyl epoxide **VEβ**, the (2-diphenylphosphanyl)phenol derivative (247 mg, 0.887mmol) was added to the solution. The epoxide formation was verified by TLC (1:1 hexane/EtOAc). After 24 hours stirring at room temperature, dilution with Et_2O and evaporation of the washed (saturated aqueous NaCl) organic solution afforded a crude mixture mostly consisting of **1β** (342 mg) which was subjected to flash chromatography. Elution with 8:2 hexane/EtOAc afforded **1β** as a white solid. Yield: 123 mg, 56 %. R_f = 0.13 (8:2 hexane/EtOAc). IR: ṽ/cm^{-1} = 3396, 3054, 2920, 2855, 1585, 1573, 1468, 1435, 1223, 1092, 1044, 741, 694. ^{1}H NMR (CDCl$_3$): δ (ppm) = 7.43-7.27 (m, 17H, Ph), 6.97 (t, $^3J_{HH}$ = 7.2 Hz, 1H, C15-H), 6.71 (ddd, $^3J_{HH}$ = 7.5, 4.5, 1.4 Hz, 1H, C13-H), 6.04 (ddd, $^3J_{HH}$ = 10.1, 4.7, 1.2 Hz, 1H, C2-H), 5.51 (s, 1H, C1-H), 5.31 (d, $^3J_{HH}$ = 10.5 Hz, 1H, C3-H), 4.56 (s, 2H, C7-H + C7-H'), 3.99-3.90 (m, 2H, C6-H + C6-H'), 3.81 (dd, $^3J_{HH}$ = 10.2, 5.0 Hz, 1H, C4-H), 3.70 (dd, $^3J_{HH}$ = 10.2, 6.7 Hz, 1H, C5-H). ^{13}C{^{1}H} NMR (CDCl$_3$): δ (ppm) = 159.0 (C12), 138.2 (C8), 136.9 (C18 + C18'), 135.2 (C16), 134.5 (C19 + C19'), 134.1 (C3), 133.8 (C14), 129.0 (C21 + C21'), 128.9 (C20 + C20'), 128.6 (C10), 128.5 (C2), 127.8 (C11), 127.6 (C9), 127.4 (C17), 123.0 (C15), 115.3 (C13), 97.6 (C1), 74.6 (C5), 73.6 (C4), 69.9 (C7), 62.8 (C6). ^{31}P{^{1}H} NMR (CDCl$_3$): δ (ppm) = - 15.4. [α]$_D^{20}$ = − 5.0° (*c* 1.26, CHCl$_3$).

(1*S*,4*S*,5*R*)-5-(Benzyloxymethyl)-4-hydroxy-1-[2-(diphenylphosphanyl)phenoxy]-2H-2,3-dihydropyran, 1α (Chart 2).

**Chart 2**. Structure of **1α** (refer to Chart S10 for C atom numbering).
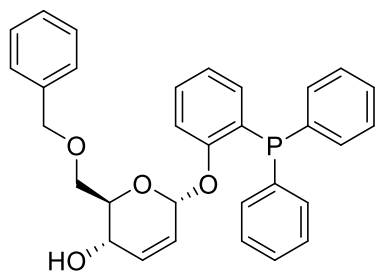
A solution of 4-*O*-mesyl-6-*O*-(benzyl)-D-gulal prepared as reported in literature,[20a] (87 mg, 0.28 mmol) in dry THF (3.0 mL) was treated with *t*-BuOK (41 mg, 0.36 mmol, 1.0 equiv) at room temperature in a Schlenk flask. After stirring for 30 minutes at the same temperature, the time necessary for the cyclization of 4-*O*-mesyl-6-*O*-(benzyl)-D-gulal to the corresponding vinyl epoxide **VEα**, the (2-diphenylphosphanyl)phenol derivative (155 mg, 0.557 mmol) was added to the solution. After 24 hours stirring at room temperature, dilution with Et₂O and evaporation of the washed (saturated aqueous NaCl) organic solution afforded a crude mixture mostly consisting of **1α** (173 mg) which was subjected to flash chromatography. Elution with 8:2 hexane/EtOAc afforded pure **1α** as a white solid. Yield: 91 mg, 66 %. R_f = 0.20 (8:2 hexane/EtOAc). IR: ṽ/cm⁻¹ = 3521, 3020, 2937, 2874, 1680, 1604, 1209, 1104, 972, 748. ¹H NMR (CDCl₃): δ (ppm) = 7.34-7.27 (m, 17H, Ph), 6.97-6.91 (m, 1H, C15-H), 6.74-6.69 (m, 1H, C13-H), 5.88 (d, $^3J_{HH}$ = 10.2 Hz, 1H, C3-H), 5.48 (s, 1H, C1-H), 5.31-5.25 (m, 1H, C2-H), 4.59 (d, $^3J_{HH}$ = 12.0 Hz, 1H, C7-H), 4.52 (d, $^3J_{HH}$ = 12.0 Hz, 1H, C7-H'), 4.19 (d, $^3J_{HH}$ = 7.2 Hz, 1H, C4-H), 3.71-3.48 (m, 3H, C5-H + C6-H + C6-H'). ¹³C{¹H} NMR (CDCl₃): δ (ppm) = 159.0 (C12), 137.9 (C8), 136.8 (C18 + C18'), 134.5 (C16), 134.2 (C19 + C19'), 133.7 (C3), 133.3 (C14), 130.3 (C21 + C21'), 128.8 (C20 + C20'), 128.6 (C10), 128.4 (C2), 127.9 (C11), 127.8 (C9), 125.0 (C17), 122.6 (C15), 115.3 (C13), 93.4 (C1), 73.7 (C5), 70.8 (C4), 70.4 (C7), 65.3 (C6). ³¹P{¹H} NMR (CDCl₃): δ (ppm) = -14.5. [α]$_D^{20}$ = − 18.6° (*c* 2.75, CHCl₃).

1-*O*-(2-azidoethyl)-2,3,4,6-tetra-*O*-acetyl-β-D-glucopyranoside (Chart 3).

Chart 3. Structure of 1-*O*-(2-azidoethyl)- 2,3,4,6-tetra-*O*-acetyl-β-D-glucopyranoside (refer to Chart S10 for C atom numbering).
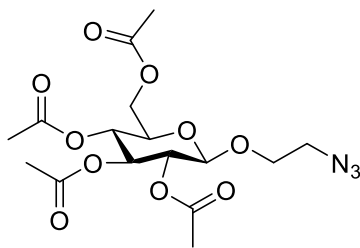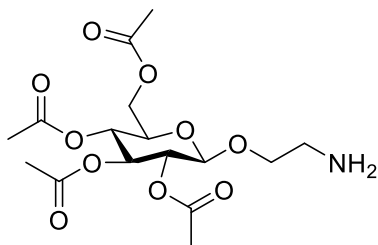
2,3,4,6-tetra-*O*-acetyl-α-D-glucopyranosyl trichloroacetimidate (150 mg, 0.304 mmol), prepared as reported in literature,[54] was dissolved in anhydrous toluene and subjected to vacuum. After complete evaporation of toluene, in order to remove residual water, vacuum-argon cycles were carried out and anhydrous DCM (6.5 mL) was added to dissolve the compound. Molecular sieves 4Å, previously activated, and a solution ~1.3 M in anhydrous DCM of the glycosyl acceptor, 2-azido-1-ethanol[29] (0.7 mL, 0.912 mmol) were added. After cooling at -20°C, a freshly prepared solution of trimethylsilyl triflate 0.1 M (0.6 mL, 0.0608 mmol, d = 1.23 g/mL) was added dropwise and the reaction mixture is stirred for 3 hours (monitoring by analytical TLC 1:1 hexane/EtOAc), at room temperature. After dilution with DCM, the mixture was quenched with TEA and filtered through a celite pad, with 95:5 DCM/MeOH as eluent. Purification by flash column chromatography, using a 6:4 hexane/EtOAc mixture as eluent, afforded pure product as a white foamy solid. Yield: 64 mg, 51 %. R_f = 0.16 (6:4 hexane/EtOAc). ^{1}H NMR (CDCl$_3$): δ (ppm) = 5.21 (t, $^3J_{HH}$ = 9.6 Hz, 1H, C3-H), 5.10 (t, $^3J_{HH}$ = 9.6 Hz, 1H, C2-H), 5.03 (t, $^3J_{HH}$ = 9.0 Hz, 1H, C4-H), 4.58 (d, $^3J_{HH}$ = 8.0 Hz, 1H, C1-H), 4.25 (dd, $^3J_{HH}$ = 12.0, 4.4 Hz, 1H, C5-H), 4.16 (dd, $^3J_{HH}$ = 12.0, 2.4 Hz, 1H, C6-H), 3.99-4.04 (m, 1H, C6-H'), 3.64-3.71 (m, 2H, C15-H + C15-H'), 3.45-3.51 (m, 1H, C16-H), 3.23-3.29 (m, 1H, C16-H'), 2.07 (s, 3H, Ac), 2.03 (s, 3H, Ac), 2.01 (s, 3H, Ac), 1.98 (s, 3H, Ac). ^{13}C{^{1}H} NMR (CDCl$_3$): δ (ppm) = 170.88, 170.50, 169.62 (C7 + C9 + C11 + C13), 100.86 (C1), 72.97 (C5), 72.10 (C3), 71.22 (C2), 68.82 (C4), 68.46 (C15), 61.70 (C6), 50.70 (C16), 20.97, 20.92, 20.83 (C8 + C10 + C12 + C14).

1-*O*-(2-aminoethyl)-2,3,4,6-tetra-*O*-acetyl-β-D-glucopyranoside (Chart 4).

Chart 4. Structure of 1-*O*-(2-aminoethyl)- 2,3,4,6-tetra-*O*-acetyl-β-D-glucopyranoside (refer to Chart S10 for C atom numbering).


1-O-(2-azidoethyl)-2,3,4,6-tetra-O-acetyl-β-D-glucopyranoside (400 mg, 0.96 mmol), was dissolved in 70 mL of MeOH for HPLC and 10% palladium hydroxide on activated charcoal (400 mg) was added. The reaction mixture is hydrogenated (1 bar) at room temperature under hydrogen saturated atmosphere until complete reduction of azide group. Conversion was checked by TLC 1:1 hexane/EtOAc. After 24 h the mixture was diluted with MeOH and filtered through a celite pad with 9:1 EtOAc/MeOH as eluent. Evaporation of the solvent afforded a crude reaction product which was not subjected to further purification processes. Yield: 350 mg, 93 %. R_f = 0.04 (95:5 EtOAc/MeOH). ^{1}H NMR (CDCl$_3$): δ (ppm) = 5.20 (t, $^3J_{HH}$ = 9.6 Hz, 1H, C3-H), 5.08 (dd, $^3J_{HH}$ = 9.6, 18.8 Hz, 1H, C2-H), 4.96 (dd, $^3J_{HH}$ = 8.0, 9.6 Hz, 1H, C4-H), 4.57 (d, $^3J_{HH}$ = 8.0 H, 1H, C1-H), 4.34 (dd, $^3J_{HH}$ = 10.4, 12.4, 1H, C5-H), 4.07-4.14 (m, 2H, C6-H + C6-H'), 3.97 (t, $^3J_{HH}$ = 4.8 Hz, 1H, C15-H), 3.72-3.77 (m, 1H, C15-H'), 3.08-3.11 (m, 2H, C16-H + C16-H'), 2.08 (s, 3H, Ac), 2.05 (s, 3H, Ac), 2.03 (s, 3H, Ac), 2.00 (s, 3H, Ac). ^{13}C{^{1}H} NMR (CDCl$_3$): δ (ppm) = 170.81, 170.25, 169.94, 169.52 (C7 + C9 + C11 + C13), 101.32 (C1), 72.66 (C5), 72.61 (C3), 72.53 (C2), 72.38 (C4), 71.15 (C15), 70.32 (C6), 40.44 (C16), 20.80, 20.78, 20.72, 20.70 (C8 + C10 + C12 + C14).

4-(Diphenylphosphanyl borane)benzoic acid, Ph₂P(BH₃)(4-C₆H₄CO₂H) (Chart 5).

Chart 5. Structure of Ph₂P(BH₃)(4-C₆H₄CO₂H) (refer to Chart S10 for C atom numbering).
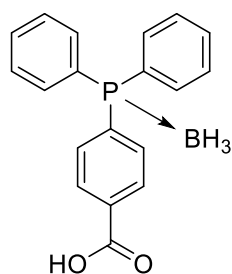
According to the literature,[55] commercial 4-(diphenylphosphanyl)benzoic acid (380 mg, 1.24 mmol) was dissolved in anhydrous THF under argon flow, and a solution of borane dimethyl sulfide (0.24 mL, 2.52 mmol) was added dropwise. The reaction was monitored by TLC 1:1 hexane/EtOAc and after 4 h, the solvent was removed under vacuum. Crude product was obtained as a colourless oil and purified by flash column chromatography, using a 1:1 hexane/EtOAc mixture as eluent. Pure product appears as a white solid. Yield: 308 mg, 80 %. R_f = 0.46 (1:1 hexane/EtOAc). ^{1}H NMR (CDCl$_3$): δ (ppm) = 11.5 (bs, 1H, COOH), 8.10 (d, $^3J_{HH}$ = 8.1 Hz, 2H, C3-H), 7.67-7.40 (m, 12H, Ph), 1.90-0.85 (bbs, 3H, BH$_3$). ^{13}C{^{1}H} NMR (CDCl$_3$): δ (ppm) = 171.39 (C5), 136.20 (C1), 133.43 (C6 + C6'), 133.34 (C2) 131.80 (C7 + C7'), 130.24 (C3 + C4), 120.19 (C8 + C8' + C9 + C9'). ^{31}P{^{1}H} NMR (CDCl$_3$): δ (ppm) = 21.4.

1-*O*-[2-(4-diphenylphosphanyl borane)-benzamide]-2,3,4,6-tetra-*O*-acetyl-β-D-glucopyranoside, 3·BH$_3$ (Chart 6).

Chart 6. Structure of **3·BH$_3$** (refer to Chart S10 for C atom numbering).
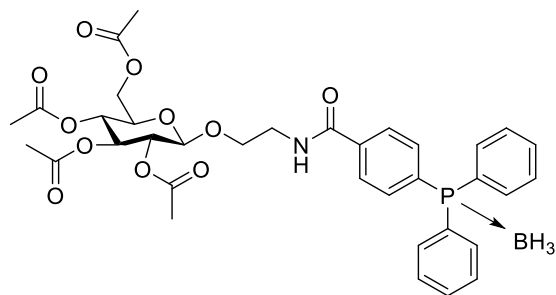

1-*O*-(2-aminoethyl)-2,3,4,6-tetra-*O*-acetyl-β-D-glucopyranoside (32 mg, 0.082 mmol) was dissolved in anhydrous DMF (0.4 mL) and 4-(diphenylphosphanyl borane)benzoic acid (25.04 mg, 0.082 mmol), HATU (32.74 mg, 0.0861 mmol) and DIPEA (0.06 mL, 0.328 mmol) were added. The reaction was carried out in a microwave reactor at 60°C for 45 minutes and monitored by TLC 1:1 hexane/EtOAc.

Workup consisted in an extraction with EtOAc (30 mL), washing the organic layer with saturated aqueous NaCl (3x5mL). The organic phase was then dried over anhydrous Na_2SO_4, filtered, and concentrated under reduced pressure. Crude product was purified by flash column chromatography using 8:2 DCM/EtOAc as eluent and the pure product was obtained as a white oil. Yield: 24 mg, 43 % yield. R_f = 0.06 (1:1 hexane/EtOAc). IR: $\tilde{\upsilon}$/cm^{-1} = 3400, 3301, 3057, 2938, 2238, 1754, 1652, 1535, 1486, 1226, 1039, 911, 846, 746, 698. ^{1}H NMR (CDCl$_3$): δ (ppm) = 7.83 (d, $^3J_{HH}$ = 7.6 Hz, 2H, C19-H), 7.66-7.42 (m, 12H, Ph), 5.20 (t, $^3J_{HH}$ = 9.4, 1H, C2-H), 5.08-4.95 (m, 2H, C3-H + C4-H), 4.53 (d, $^3J_{HH}$ = 7.9 Hz, 1H, C1-H), 4.22 (dd, $^3J_{HH}$ = 12.4, 4.8 Hz, 1H, C5-H), 4.11 (dd, $^3J_{HH}$ = 14.1, 7.18 Hz, 2H, C6-H + C6-H'), 3.96-3.91 (m, 1H, C15-H), 3.83-3.63 (m, 3H, C16-H + C16-H' + C15-H'), 2.03 (s, 3H, Ac), 2.01 (s, 3H, Ac), 2.00 (s, 3H, Ac), 1.99 (s, 3H, Ac). ^{13}C{^{1}H} NMR (CDCl$_3$): δ (ppm) = 171.1, 170.5, 170.1, 169.5 (C7 + C9 + C11 + C13), 166.5 (C17), 136.8 (C21), 136.7 (C22 + C22'), 133.2 (C20 + C23 + C23') 133.1 (C18), 129.0 (C24 + C24' + C25 + C25'), 127.2 (C19), 100.9 (C1), 72.7 (C5), 72.1 (C3), 71.4 (C2), 68.8 (C4), 68.3 (C15), 60.4 (C6), 39.7 (C16), 20.5 (C8 + C10 + C12 + C14). ^{31}P{^{1}H} NMR (CDCl$_3$): δ (ppm) = 21.00. $[\alpha]_D^{20}$ = − 13.3° (c 2.3, CHCl$_3$).

1-*O*-[2-(4-diphenylphosphanyl borane) benzamide]-β-D-glucopyranoside, 4·BH₃ (Chart 7).

Chart 7. Structure of **4·BH₃** (refer to Chart S10 for C atom numbering).
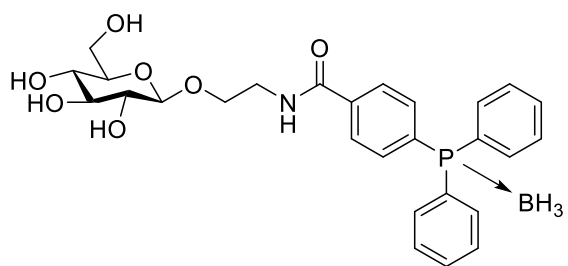

1-O-[2-(4-diphenylphosphanyl borane)benzamide]-2,3,4,6-tetra-O-acetyl-β-D-glucopyranoside (**3·BH₃**) (24 mg, 0.035 mmol) was dissolved in MeOH and a freshly prepared solution of MeONa in MeOH (0.33M) was added dropwise (0.64 mL, 0.21 mmol). This latter solution was prepared by dissolving Na metal in MeOH. The reaction mixture was stirred for 2 h at room temperature, monitoring by TLC 1:1

hexane/EtOAc. When conversion was complete, Amberlite® IR120 resin was added for quenching and the mixture was stirred until neutral pH value. Resin was then removed by filtration and, after evaporation of the solvent under reduced pressure, pure product was obtained as a colourless oil. Yield: 17 mg, 90 %. The isolated product contains small impurities ascribable to the free phosphane (**4**) and its oxide (**4O**). R_f = 0.17 (9:1 DCM/MeOH). IR: $\tilde{\nu}$/cm^{-1} = 3509, 3483, 3433, 3401, 3389, 3266, 3240, 2901, 2848, 2795, 2242, 2075, 1621, 1556, 1425, 1337, 1102, 1082, 976, 824. ^{1}H NMR (CD$_3$OD): δ (ppm) = 7.90 (d, $^3J_{HH}$ = 7.8 Hz, 2H, C11-H), 7.67-7.47 (m, 12H, Ph), 4.31 (d, $^3J_{HH}$ = 7.6 Hz, 1H, C1-H), 4.07-4.02 (m, 1H, C2-H), 3.85 (d, $^3J_{HH}$ = 11.4 Hz, 1H, C6-H), 3.80-3.73 (m, 1H, C7-H), 3.73-3.63 (m, 1H, C6-H'), 3.63-3.49 (m, 2H, C8-H + C8-H'), 3.37-3.33 (m, 1H, C3-H), 3.33-3.28 (m, 2H, C5-H, C4-H), 3.28-3.20 (m, 1H, C7-H'). ^{13}C{^{1}H} NMR (CD$_3$OD): δ (ppm) = 168.0 (C9), 137.1 (C13), 132.9 (C14 + C14'), 132.8 (C12 + C15 + C15'), 131.3 (C10), 128.7 (C16 + C16' + C17 + C17'), 128.6 (C11), 103.2 (C1), 76.6 (C5), 76.6 (C3), 73.7 (C2), 70.2 (C4), 68.0 (C7), 61.3 (C6), 39.9 (C8). ^{31}P{^{1}H} NMR (CD$_3$OD): δ (ppm) = 20.59 (**4·BH$_3$**, NMR purity = 95%), 31.47 (**4O**), -5.75 (**4**). $[\alpha]_D^{20}$ = − 10.9° (*c* 2.0, CH$_3$OH).

3. Synthesis and characterization of glycoconjugated ruthenium complexes.

[Ru(C$_2$O$_4$)(η^6-*p*-cymene)(H$_2$O)] (Chart 8).

**Chart 8**. Structure of [Ru(C$_2$O$_4$)(η^6-*p*-cymene)(H$_2$O)], **Ru-H$_2$O** (refer to Chart S10 for C atom numbering).
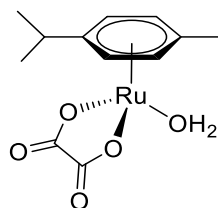
The title compound was prepared as described in the literature from AgNO$_3$ (742 mg, 4.37 mmol), Na$_2$C$_2$O$_4$ (292 mg, 2.18 mmol) and [RuCl$_2$(η^6-*p*-cymene)]$_2$ (222 mg, 0.725 mmol).[56] Yield: 236 mg, 95 %. Canary yellow solid, stored under N$_2$ at 4 °C.[57] Soluble in DMSO, water, MeOH, CH$_2$Cl$_2$ and

CHCl$_3$, insoluble in acetone and Et$_2$O. A single crystal of [Ru(C$_2$O$_4$)(η^6-p-cymene)(H$_2$O)]·2H$_2$O suitable for X-ray diffraction was grown by slow evaporation of an aqueous solution at room temperature. ^{1}H NMR (D$_2$O): δ (ppm) = 5.84 (d, $^3J_{HH}$ = 6.2 Hz, 2H, C4-H), 5.60 (d, $^3J_{HH}$ = 6.2 Hz, 2H, C3-H), 2.86 (hept, $^3J_{HH}$ = 6.9 Hz, 1H, C6-H), 2.23 (s, 3H, C1-H), 1.32 (d, $^3J_{HH}$ = 6.9 Hz, 6H, C7-H). ^{1}H NMR (CD$_3$OD): δ (ppm) = 5.81 (d, $^3J_{HH}$ = 6.2 Hz, 2H, C4-H), 5.57 (d, $^3J_{HH}$ = 6.1 Hz, 2H, C3-H), 2.91 (hept, $^3J_{HH}$ = 6.9 Hz, 1H, C6-H), 2.28 (s, 3H, C1-H), 1.39 (d, $^3J_{HH}$ = 6.9 Hz, 6H, C7-H). ^{1}H NMR (CDCl$_3$): δ (ppm) = 5.81, 5.46, 5.41, 5.18 (d, $^3J_{HH}$ = 5.7 Hz, 4H, C4-H + C3-H), 2.92–2.81 (m, 1H, C6-H), 2.24 (s, 3H, C1-H), 1.23 (d, $^3J_{HH}$ = 6.9 Hz, 6H, C7-H).

[Ru(C$_2$O$_4$)(η^6-p-cymene)(1β)], Ru1β (Chart 9).

Chart 9. Structure of **Ru1β** (refer to Chart S10 for C atom numbering).
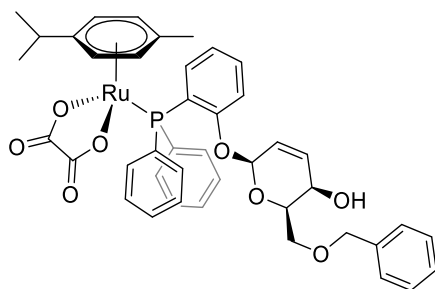
In a 25-mL Schlenk tube under N$_2$, a yellow solution of [Ru(C$_2$O$_4$)(η^6-p-cymene)(H$_2$O)] (62 mg, 0.182 mmol) and **1β** (91 mg, 0.183 mmol) in anhydrous CH$_2$Cl$_2$ (10 mL) was stirred at room temperature for 4 hours. The conversion was checked by ^{31}P{^{1}H} NMR then the solution was concentrated under vacuum and moved on top of a silica column (h 6, d 2.3 cm). Impurities were eluted with CH$_2$Cl$_2$:acetone 7:1 *v/v* then a yellow band was collected using CH$_2$Cl$_2$:EtOH 5:2 *v/v*. Volatiles were removed under vacuum and the residue was suspended in Et$_2$O. The suspension was filtered and the resulting yellow solid was washed with Et$_2$O and dried under vacuum. Yield: 122 mg, 82 %. Soluble in DMSO, CH$_2$Cl$_2$, CHCl$_3$, MeOH, acetone, insoluble in Et$_2$O and water. Anal. Calcd. for C$_{43}$H$_{43}$O$_8$PRu: C, 63.00; H, 5.29. Found: C, 62.5; H, 5.20. IR: ṽ/cm^{-1} = 3340w-br (ν$_{OH}$), 3060w, 3023w, 2964w,

2923w, 2867w, 2164w, 1983w; 1693s, 1671s, 1648s-sh ($v_{C=O}$); 1586m, 1575m-sh, 1471m, 1436s, 1372s, 1324m, 1278m, 1233m, 1183m, 1094s, 1080m-sh, 1044s, 1001m, 898m, 853m, 803w, 783m, 746s, 696s. ^{1}H NMR (CDCl$_3$): δ (ppm) = 7.75 (dd, $^3J_{HP}$ = 12.4 Hz, $^3J_{HH}$ = 7.7 Hz, 1H, C14-H), 7.55 (t, $^3J_{HH}$ = 7.6 Hz, 1H, C16-H), 7.46 (dd, $^3J_{HH}$ = 8.3 Hz, $^4J_{HP}$ = 3.8 Hz, 1H, C17-H), 7.43–7.27 (m, 15H, Ph), 7.18 (t, $^3J_{HH}$ = 7.4 Hz, 1H, C15-H), 5.91 (dd, $^3J_{HH}$ = 9.8, 4.1 Hz, 1H, C21-H), 5.49 (d, $^3J_{HH}$ = 6.0 Hz, 1H, C4'-H), 5.45 (s, 1H, C19-H), 5.41 (d, $^3J_{HH}$ = 5.7 Hz, 1H, C4-H), 5.16 (d, $^3J_{HH}$ = 5.7 Hz, 1H, C3-H), 4.91 (d, $^3J_{HH}$ = 6.0 Hz, 1H, C3'-H), 4.69 (d, $^3J_{HH}$ = 10.1 Hz, 1H, C20-H), 4.54 (pseudo-q, $^1J_{HH}$ = 12 Hz, 2H, C25-H + C25-H'), 3.90–3.83 (m, 2H, C22-H + C23-H), 3.68–3.61 (m, 2H, C24-H + C24-H'), 2.67 (hept, $^3J_{HH}$ = 6.9 Hz, 1H, C6-H), 2.55 (s-br, 1H, OH), 1.91 (s, 3H, C1-H), 1.20 (d, $^3J_{HH}$ = 6.9 Hz, 3H, C7-H), 1.11 (d, $^3J_{HH}$ = 6.8 Hz, 3H, C7'-H). ^{13}C{^{1}H} NMR (CDCl$_3$): δ (ppm) = 165.3 (C8), 164.8 (C8'), 158.4 (C18), 138.2 (C26), 136.9 (d, $^2J_{CP}$ = 13 Hz, C14), 134.2 (C16), 133.9 (d, $^2J_{CP}$ = 10 Hz, C10), 133.1 (d, $^2J_{CP}$ = 10 Hz, C10'), 131.3 (C21), 130.8 (d, $^4J_{CP}$ = 2 Hz, C12), 130.7 (d, $^1J_{CP}$ = 48 Hz, C9'), 130.6 (d, $^4J_{CP}$ = 2 Hz, C12'), 128.7 (d, $^3J_{CP}$ = 10 Hz, C11), 128.6 (C27), 128.5 (d, $^3J_{CP}$= 11 Hz, C11'), 128.1 (C20), 127.9 (C29), 127.7 (C28), 122.6 (d, $^3J_{CP}$ = 11 Hz, C15), 118.4 (d, $^1J_{CP}$ = 46 Hz, C13), 115.5 (d, $^3J_{CP}$ = 4 Hz, C17), 108.1 (d, $^2J_{CP}$ = 3 Hz, C5), 97.5 (C2), 95.5 (C19), 88.5 (d, $^2J_{CP}$ = 4 Hz, C3'), 87.7 (d, $^2J_{CP}$ = 4 Hz, C4'), 87.1 (d, $^2J_{CP}$ = 4 Hz, C4), 85.3 (C3), 74.9 (C23), 73.6 (C25), 69.8 (C24), 62.2 (C22), 30.8 (C6), 22.9 (C7), 22.0 (C7'), 18.0 (C1). ^{31}P{^{1}H} NMR (CDCl$_3$): δ (ppm) = 27.5. $[α]_D^{20}$ = − 67.4° (c 0.34, MeOH).

[Ru(C$_2$O$_4$)(η^6-*p*-cymene)(1α)], Ru1α (Chart 10).

Chart 10. Structure of **Ru1α** (refer to Chart S10 for C atom numbering).
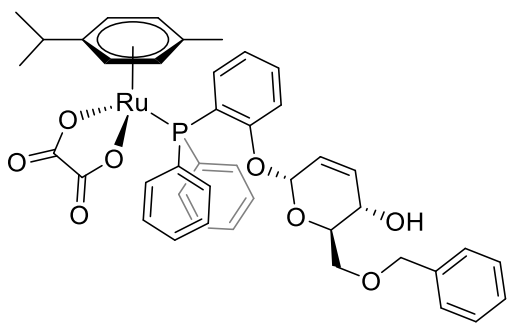
The compound was prepared as described for **Ru1β**, using [Ru(C$_2$O$_4$)(η^6-p-cymene)(H$_2$O)] (32 mg, 0.093 mmol) and **1α** (52 mg, 0.10 mmol). Silica chromatography: impurities eluted with CH$_2$Cl$_2$:acetone 7:3 v/v then a yellow band eluted using CH$_2$Cl$_2$:EtOH 5:2 v/v. Yellow solid; Yield: 70 mg, 91 %. Soluble in DMSO, CH$_2$Cl$_2$, CHCl$_3$, MeOH, insoluble in acetone, Et$_2$O and water. Anal. Calcd. for C$_{43}$H$_{43}$O$_8$PRu: C, 63.0; H, 5.29. Found: C, 61.8; H, 5.15. IR: ṽ/cm^{-1} = 3301w-br (v_{OH}), 3064w, 2964w, 2913w, 2868w; 1694s, 1670s, 1641s ($v_{C=O}$); 1586m, 1511w, 1498w, 1471m, 1441m, 1435m, 1377s, 1338w, 1324w, 1281m, 1234m, 1185w, 1163w, 1156w, 1137w, 1117m, 1103m, 1095m, 1088m, 1072m, 1054m, 1027m, 998w, 981m, 952s, 945s, 876w, 844w, 805w, 785m, 751m-sh, 745s, 697s. ^{1}H NMR (CD$_3$OD): δ (ppm) = 8.05 (dd, $^3J_{HH}$ = $^3J_{HP}$ = 7.1 Hz, 1H, C14-H), 7.69 (t, $^3J_{HH}$ = 7.7 Hz, 1H, C16-H), 7.51 (dd, $^3J_{HH}$ = 8.3 Hz, $^4J_{HP}$ = 3.5 Hz, 1H, C17-H), 7.49–7.19 (m, 16H, Ph + C15-H), 5.72 (d, $^3J_{HH}$ = 5.6 Hz, 1H, C4-H), 5.67–5.63 (m, 2H, C4'-H + C21-H), 5.38 (s, 1H, C19-H), 5.34 (d, $^3J_{HH}$ = 5.2 Hz, 1H, C3'-H), 5.14 (d, $^3J_{HH}$ = 5.4 Hz, 1H, C3-H), 4.49–4.41 (m, 3H, C20-H + C25-H + C25-H'), 3.86 (d, $^3J_{HH}$ = 8.5 Hz, 1H, C22-H), 3.65 (dd, $^2J_{HH}$ = 11.1 Hz, $^3J_{HH}$ = 1.4 Hz, 1H, C24-H), 3.53 (d, $^2J_{HH}$ = 11.2 Hz, 1H, C24-H'), 3.14–3.06 (m, 1H C23-H), 2.61 (hept, $^3J_{HH}$ = 6.7 Hz, 1H, C6-H), 1.92 (s, 3H, C1-H), 1.23 (d, $^3J_{HH}$ = 6.9 Hz, 3H, C7-H), 1.18 (d, $^3J_{HH}$ = 6.8 Hz, 3H, C7'-H). ^{13}C{^{1}H} NMR (CD$_3$OD): δ (ppm) = 167.1 (C8), 166.9 (C8'), 160.4 (d, $^2J_{CP}$ = 1 Hz, C18), 139.9 (d, $^2J_{CP}$ = 18 Hz, C14), 139.7 (C26), 136.1 (C21), 136.0 (d, $^4J_{CP}$ = 1 Hz, C16), 134.0 (d, $^2J_{CP}$ = 10 Hz, C10/C10'), 133.8 (d, $^2J_{CP}$ = 10 Hz, C10/C10'), 131.7 (d, $^4J_{CP}$ = 2 Hz, C12/C12'), 131.4 (d, $^4J_{CP}$ = 2 Hz, C12/C12'), 131.4 (d, $^1J_{CP}$ = 48 Hz, C9/C9'), 130.4 (d, $^1J_{CP}$ = 47 Hz, C9/C9'), 129.7 (d, $^3J_{CP}$ = 11 Hz, C11/C11'), 129.6 (d, $^3J_{CP}$ = 11 Hz, C11/C11'), 129.3 (C28), 128.6 (C27), 128.5 (C29), 124.6 (C20),

123.1 (d, $^3J_{CP}$ = 13 Hz, C15), 117.6 (d, $^1J_{CP}$ = 48 Hz, C13), 116.9 (d, $^3J_{CP}$ = 3 Hz, C17), 109.3 (d, $^2J_{CP}$ = 3 Hz, C5), 99.3 (C2), 94.4 (C19), 89.2 (d, $^2J_{CP}$ = 4 Hz, C4), 88.9 (d, $^2J_{CP}$ = 3 Hz, C3/C4'), 88.7 (d, $^2J_{CP}$ = 4 Hz, C3/C4'), 86.6 (d, $^2J_{CP}$ = 1 Hz, C3'), 74.1 (C25), 74.0 (C23), 70.6 (C24), 63.8 (C22), 32.2 (C6), 22.8 (C7), 22.2 (C7'), 18.1 (C1). $^{31}P\{^1H\}$ NMR (CD$_3$OD): δ (ppm) = 29.7. ^1H NMR (CDCl$_3$): δ (ppm) = 7.90 (dd, $^3J_{HP}$ = 12.8 Hz, $^3J_{HH}$ = 7.7 Hz, 1H, C14-H), 7.58 (t, $^3J_{HH}$ = 7.2 Hz, 1H, C16-H), 7.52–7.19 (m, 17H, Ph + C15-H + C17-H), 5.70 (d, $^3J_{HH}$ = 9.7 Hz, 1H, C21-H), 5.46 (m-br, 1H, C4-H/C4'-H), 5.36 (s, 1H, C19-H), 5.33 (m-br, 1H, C4-H/C4'-H), 5.09 (m-br, 1H, C3-H/C3'-H), 4.88 (m-br, 1H, C3-H/C3'-H), 4.56–4.47 (m, 3H, C20-H + C25-H + C25-H'), 3.99 (d, $^3J_{HH}$ = 8.6 Hz, 1H, C22-H), 3.78–3.71 (m, 1H, C24-H/C24-H'), 3.66–3.51 (m, 2H, C24-H/C24-H' + C23-H), 3.35 (br, 1H, OH), 2.62 (m, C6-H),* 1.80 (s, 3H, C1-H), 1.26–1.20 (m, 6H, C7-H + C7'-H). *Over H$_2$O peak. $^{31}P\{^1H\}$ NMR (CDCl$_3$): δ (ppm) = 25.2. [α]$_D^{20}$ = − 12.5° (c 0.38, MeOH).

[Ru(C$_2$O$_4$)(η^6-p-cymene)(2β)], Ru2β (Chart 11).

Chart 11. Structure of **Ru2β** (refer to Chart S10 for C atom numbering).
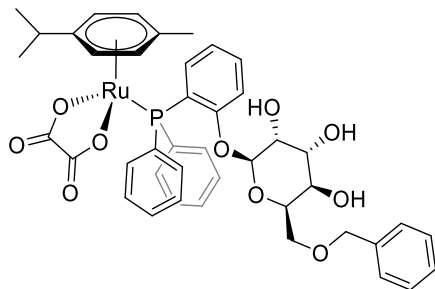
In a 5-mL test tube, **Ru1β** (36 mg, 0.044 mmol) was dissolved in a mixture of ^{t}BuOH (0.25 mL) and acetone (0.25 mL). The golden yellow solution was cooled to 0°C then treated with N-methylmorpholine-N-oxide (50% m/V solution in H$_2$O, 40 μL, 0.17 mmol) and OsO$_4$ (2.5 %wt. solution in ^{t}BuOH, 55 μL, 4.4 μmol). The solution was stirred at 0 °C in the dark for 8.5 h then moved on top of a silica column (h 6, d 2.3 cm). Impurities were eluted with CH$_2$Cl$_2$:EtOH 4:1 v/v then a yellow band was collected using MeOH. Volatiles were removed under vacuum; the residue was

dissolved in CH_2Cl_2 and filtered over celite. The filtrate was taken to dryness under vacuum and the residue was suspended in Et_2O. The suspension was filtered and the resulting yellow solid was washed with Et_2O and dried under vacuum. Yield: 28 mg, 75 %. Soluble in DMSO, CH_2Cl_2, $CHCl_3$, MeOH, poorly soluble in water and insoluble in Et2O. Anal. Calcd. for $C_{43}H_{45}O_{10}PRu$: C, 60.49; H, 5.31. Found: C, 60.1; H, 5.24. IR: $\tilde{\upsilon}/cm^{-1}$ = 3600-3200w-br (ν_{OH}), 3065w, 2966w, 2919w, 2874w; 1693m-sh, 1651s, 1633s-sh ($\nu_{C=O}$); 1586m, 1574w, 1472m-sh, 1435s, 1391m, 1318m, 1282m, 1233m, 1090s, 1073s, 1051s, 999m-sh, 909w, 823w, 792w, 749m, 697s. ^1H NMR (CD_3OD): δ (ppm) = 7.70–7.50 (m, 7H, Ph), 7.37–7.31 (m, 1H, C16-H), 7.31–7.14 (m, 9H, Ph), 6.94 (app. t, J = 8.6 Hz, 2H, C10-H), 6.31 (d, $^3J_{HH}$ = 5.8 Hz, 1H, C4-H), 6.03 (d, $^3J_{HH}$ = 5.4 Hz, 1H, C4'-H), 5.74 (d, $^3J_{HH}$ = 8.1 Hz, 1H, C19-H), 5.60 (s-br, 1H, C3'-H), 4.61 (d, $^2J_{HH}$ = 12.0 Hz, 1H, C25-H), 4.51 (d, $^2J_{HH}$ = 12.0 Hz, 1H, C25-H'), 4.46–4.38 (m, 2H, C3-H + C23-H), 4.29–4.24 (m, 1H, C20-H), 4.08–4.04 (m, 1H, C21-H), 3.86 (d, J = 2.7 Hz, 1H, C22-H), 3.81–3.71 (m, 2H, C24-H + C24-H'), 2.93 (hept, $^3J_{HH}$ = 6.5 Hz, 1H, C6-H), 1.74 (s, 3H, C1-H), 1.24 (d, $^3J_{HH}$ = 6.9 Hz, 3H, C7-H), 1.20 (d, $^3J_{HH}$ = 6.7 Hz, 3H, C7-H'). $^{13}C\{^1H\}$ NMR (CD_3OD): δ (ppm) = 167.9, 167.7 (C8 + C8'); 159.6 (d, $^2J_{CP}$ = 6 Hz, C18), 139.7 (C26), 138.3 (d, $^2J_{CP}$ = 12 Hz, C14), 135.2, 134.9 (d, $^2J_{CP}$ = 10 Hz, C10 + C10'); 134.7 (d, $^4J_{CP}$ = 1 Hz, C16), 132.9, 131.3 (C12 + C12'); 130.0 (d, $^1J_{CP}$ = 47 Hz, C9/C9'); 130.0, 129.6 (d, $^3J_{CP}$ = 10 Hz, C11 + C11'); 129.3 (C28), 129.2 (d, $^1J_{CP}$ = 49 Hz, C9/C9'), 128.7 (C27), 128.6 (C29), 122.9 (d, $^3J_{CP}$ = 8 Hz, C15), 120.8 (d, $^1J_{CP}$ = 47 Hz, C13), 116.2 (d, $^3J_{CP}$ = 9 Hz, C16), 116.0 (d, $^2J_{CP}$ = 5 Hz, C5), 99.2 (C2), 98.0 (C19), 91.6 (s-br, C4'), 87.7 (C3), 87.0 (C4), 81.9 (s-br, C3'), 74.2 (C25), 74.0 (C23), 73.6 (C21), 71.2, 71.1 (C22 + C24); 67.9 (C20), 32.0 (C6), 23.6 (C7), 20.8 (C7'), 18.5 (C1). $^{31}P\{^1H\}$ NMR (CD_3OD): δ (ppm) = 33.6. $[\alpha]_D^{20}$ = $-$ 71.8° (c 0.17, MeOH).

[Ru(C_2O_4)(η^6-p-cymene)(2α)], Ru2α (Chart 12).

Chart 12. Structure of **Ru2α** (refer to Chart S10 for C atom numbering).
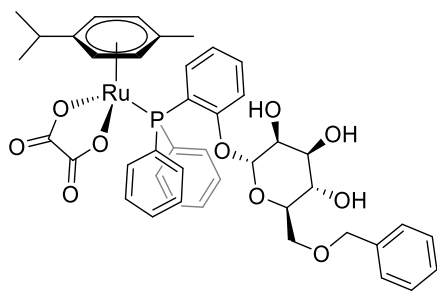
In a 5-mL test tube, **Ru1α** (35 mg, 0.042 mmol) was dissolved in the minimum amount of CH_2Cl_2 then diluted with ^tBuOH (0.25 mL) and acetone (0.20 mL). The yellow suspension was cooled to 0°C then treated with N-methylmorpholine-N-oxide (50% m/V solution in H_2O, 40 µL, 0.17 mmol) and OsO_4 (2.5 %wt. solution in ^tBuOH, 55 µL, 4.4 µmol). The solution was stirred at 0 °C in the dark for 14 h then moved on top of a silica column (h 6, d 2.3 cm). Impurities were eluted with CH_2Cl_2:EtOH 6:1 *v/v* then a yellow band was collected using MeOH/EtOH mixtures. Volatiles were removed under vacuum; the residue was dissolved in CH_2Cl_2 and filtered over celite. The filtrate was taken to dryness under vacuum and the residue was suspended in Et_2O. The suspension was filtered and the resulting yellow solid was washed with Et_2O and dried under vacuum. Yield: 23 mg, 64 %. Soluble in DMSO, CH_2Cl_2, $CHCl_3$, MeOH, appreciably soluble in water and insoluble in Et2O. Anal. Calcd. for $C_{43}H_{45}O_{10}PRu$: C, 60.49; H, 5.31. Found: C, 59.8; H 5.22. IR: $\tilde{\nu}/cm^{-1}$ = 3600-3200w-br (ν_{OH}), 3062w, 2964w, 2924w, 2868w; 1692m-sh, 1652s, 1634s-sh ($\nu_{C=O}$); 1586m, 1572m, 1470m, 1436s, 1392s-br, 1318s, 1280m, 1233m, 1142m-sh, 1121m-sh, 1092s, 1071s, 1056m, 1027m, 996m, 965s, 880w, 841w, 826w, 792m, 748m, 697s. ^1H NMR (CD$_3$OD): δ (ppm) = 8.10 (dd, $^3J_{HP}$ = 15.6 Hz, $^3J_{HH}$ = 7.1 Hz, 1H, C14-H), 7.69 (t, $^3J_{HH}$ = 7.8 Hz, 1H, C16-H), 7.54 (dd, $^3J_{HH}$ = 8.4 Hz, $^4J_{HP}$ = 3.2 Hz, 1H, C15-H), 7.52–7.34 (m, 11H, C15-H + Ph), 7.32–7.25 (m, 5H, Ph), 5.71–5.65 (m, 2H, C4-H + C4'-H), 5.26 (d, $^3J_{HH}$ = 5.7 Hz, 1H, C3-H), 5.18 (d, $^3J_{HH}$ = 5.3 Hz, 1H, C3'-H), 5.08 (s, 1H, C19-H), 4.54–4.44 (m, 2H, C25-H + C25-H'), 3.69 (d, $^2J_{HH}$ = 11.0 Hz, $^3J_{HH}$ = 1.7 Hz, 1H, C24-H'), 3.57 (dd, $^2J_{HH}$ = 11.1 Hz, $^3J_{HH}$ = 6.6 Hz, 1H, C24-H), 3.37–3.33 (m, 1H, C22-H), 3.17–3.09 (m, 1H, C23-H), 2.65–2.59 (m, 1H, C6-H), 2.59–2.55 (m, 1H, C20-H), 2.44 (dd, $^3J_{HH}$ = 9.5, 3.2 Hz, 1H, C21-H), 1.91 (s, 3H, C1-H), 1.29–1.24 (m, 6H, C7-H +

C7'-H). ^{13}C{^{1}H} NMR (CD$_3$OD): δ (ppm) = 167.2, 167.1 (C8 + C8'); 160.0 (C18), 141.9 (d, $^2J_{CP}$ = 20 Hz, C14), 139.7 (C26), 136.5 (C16), 133.5, 133.1 (d, $^2J_{CP}$ = 10 Hz, C10 + C10'); 132.1, 131.7 (C12 + C12'), 131.1 (d, $^1J_{CP}$ = 48 Hz, C9/C9'), 130.1 (app. t, $^3J_{CP}$ = 11 Hz, C11 + C11'), 129.3 (C28), 128.8 (C27), 128.6 (C29), 123.4 (d, $^3J_{CP}$ = 14 Hz, C15), 117.0 (d, $^3J_{CP}$ = 3 Hz, C17), 116.9 (d, $^1J_{CP}$ = 49 Hz, C13), 110.3 (d, $^2J_{CP}$ = 3 Hz, C5), 101.1 (C19), 99.5 (C2), 88.7, 88.4 (d, $^2J_{CP}$ = 3 Hz, C4 + C4'); 88.2 (C3'), 87.5 (C3), 74.7 (C23), 74.2 (C25), 71.5 (C21), 71.1 (C24), 70.6 (C20), 68.0 (C22), 32.3 (C6); 22.6, 22.4 (C7 + C7'), 18.1 (C1). ^{31}P{^{1}H} NMR (CD$_3$OD): δ (ppm) = 30.7. [α]$_D^{20}$ = − 101.6° (c 0.06, MeOH).

[Ru(C$_2$O$_4$)(η^6-*p*-cymene)(3)], Ru3 (Chart 13).

Chart 13. Structure of **Ru3** (refer to Chart S10 for C atom numbering).
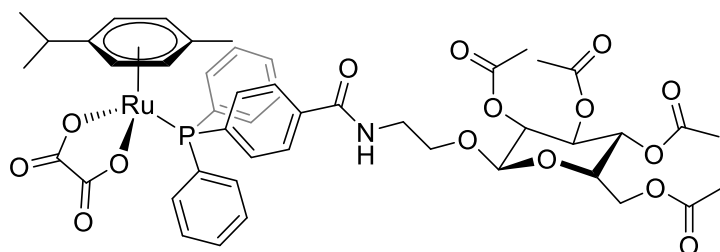
In a 25-mL Schlenk tube under N$_2$, a yellow solution of [Ru(C$_2$O$_4$)(η^6-*p*-cymene)(H$_2$O)] (16 mg, 0.045 mmol) and **3·BH$_3$** (26 mg, 0.039 mmol) in deaerated MeOH (10 mL) was stirred at 50 °C. After 17 hours, conversion was checked by ^{31}P{^{1}H} NMR and volatiles were removed under vacuum. The residue was dissolved in CH$_2$Cl$_2$ and moved on top of a silica column (h 6, d 1.2 cm). Impurities were eluted with CH$_2$Cl$_2$:acetone 7:1 *v/v* then a yellow band was collected using MeOH. Volatiles were removed under vacuum; the residue was dissolved in CH$_2$Cl$_2$ and extracted with H$_2$O (x 3). The organic phase was filtered over celite and taken to dryness under vacuum. The residue was suspended in Et$_2$O and the suspension was filtered. The resulting yellow solid was washed with Et$_2$O and dried under vacuum. Yield: 24 mg, 62 % (with respect to **3·BH$_3$**). Soluble in DMSO, CH$_2$Cl$_2$, CHCl$_3$, MeOH, sparingly soluble in water and insoluble in Et$_2$O. Anal. Calcd. for C$_{47}$H$_{52}$NO$_{15}$PRu: C: 52.28,

H, 5.22; N, 1.40. Found: C: 53.7, H, 5.55; N, 1.26. IR: $\tilde{\upsilon}$/cm^{-1} = 3600-3200w-br (ν_{NH}), 3059w, 2964w, 2934w-sh, 2877w, 1748s ($\nu_{C=O,ester}$); 1693s, 1671s, 1652-1646s ($\nu_{C8=O}$ + $\nu_{C17=O}$); 1601w-sh, 1552w, 1435m, 1368s, 1310w, 1218s, 1169m-sh, 1120m, 1094m-sh, 1061m-sh, 1034s, 1001m-sh, 982m-sh, 907w, 834w, 784m, 752w, 722w. ^{1}H NMR (CD$_3$OD): δ (ppm) = 7.81 (dd, $^3J_{HH}$ = 8.2 Hz, $^4J_{HP}$ = 1.6 Hz, 2H, C15-H), 7.64–7.53 (m, 10H, Ph), 7.46 (dd, $^3J_{HP}$ = 10.1 Hz, $^4J_{HP}$ = 8.6 Hz, 2H, C14-H), 5.76 (d, $^3J_{HH}$ = 6.1 Hz, 2H, C4-H), 5.46 (d, $^3J_{HH}$ = 6.1 Hz, 2H, C3-H), 5.24 (t, $^3J_{HH}$ = 9.5 Hz, 1H, C22-H), 5.00 (t, $^3J_{HH}$ = 9.7 Hz, 1H, C27-H), 4.92–4.87 (m, 1H, C21-H), 4.72 (d, $^3J_{HH}$ = 8.0 Hz, 1H, C20-H), 4.22 (dd, $^2J_{HH}$ = 12.3 Hz, $^3J_{HH}$ = 4.8 Hz, 1H, C25-H), 4.07 (dd, $^2J_{HH}$ = 12.2 Hz, $^3J_{HH}$ = 1.9 Hz, 1H, C25-H'), 3.99–3.92 (m, 1H, C19-H'), 3.90–3.85 (m, 1H, C24-H), 3.84–3.77 (m, 1H, C19-H), 3.57–3.50 (m, 1H, C18-H), 2.59 (hept, $^3J_{HH}$ = 6.8 Hz, 1H, C6-H); 2.00 (s, 3H), 1.98 (s, 3H), 1.95 (m-br, 6H) (C27-H + C29-H + C31-H + C33-H); 1.91 (s, 3H, C1-H), 1.23 (d, $^3J_{HH}$ = 6.9 Hz, 6H, C7-H). ^{13}C{^{1}H} NMR (CD$_3$OD): δ (ppm) = 172.2, 171.6, 171.3, 171.2 (C26 + C28 + C30 + C32); 169.2 (C17), 167.0 (C8), 138.2 (C16), 135.5 (d, $^2J_{CP}$ = 10 Hz, C10), 135.3 (d, $^2J_{CP}$ = 10 Hz, C14), 134.3 (d, $^1J_{CP}$ = 44 Hz, C13), 132.7 (C12), 130.6* (C8), 130.2 (d, $^3J_{CP}$ = 10 Hz, C11), 128.6 (d, $^3J_{CP}$ = 10 Hz, C15), 109.3 (C5), 101.8 (C20), 99.5 (C2), 89.3 (C4), 88.1 (C3), 74.3 (C22), 72.9 (C21 + C24), 69.9 (C23), 69.2 (C19), 63.2 (C25), 41.1 (C18), 32.3 (C6), 22.5 (C7); 20.6, 20.5 (C27 + C29 + C31 + C33), 18.1 (C1). ^{31}P{^{1}H} NMR (CD$_3$OD): δ (ppm) = 32.3.

[Ru(C$_2$O$_4$)(η^6-p-cymene)(4)], Ru4 (Chart 14).

Chart 14. Structure of **Ru4** (refer to Chart S10 for C atom numbering).
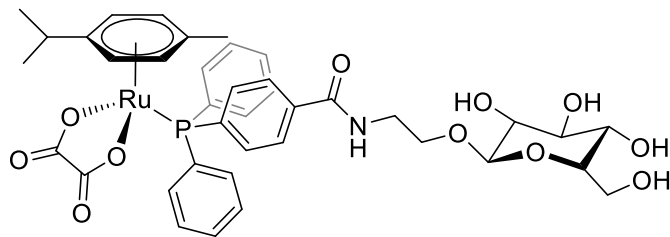
In a 25-mL Schlenk tube under N_2, a yellow solution of $[Ru(C_2O_4)(\eta^6\text{-}p\text{-cymene})(H_2O)]$ (19 mg, 0.056 mmol) and **4·BH₃** (30 mg, 0.057 mmol) in deaerated MeOH (10 mL) was stirred at 50 °C. After 21 hours, conversion was checked by $^{31}P\{^1H\}$ NMR and volatiles were removed under vacuum. The residue was dissolved in CH_2Cl_2 and moved on top of a silica column (h 3, d 2.4 cm). Impurities were eluted with acetone/MeOH 3:1 *v/v* (+ 0.25 % Et₃N) then a yellow band was collected using acetone/MeOH/Et₃N 1:1 (+ 0.25 % Et₃N). Volatiles were removed under vacuum; the residue was suspended in MeCN and filtered over celite. The filtrate was dried under vacuum and the residue was triturated in a small volume of cold acetone (-20 °C). The suspension was filtered; the resulting yellow solid was washed with Et₂O and dried under vacuum. Yield: 33 mg, 70 % (with respect to **4·BH₃**). Soluble in H_2O, DMSO, CH_2Cl_2, MeOH, insoluble in EtOAc, Et₂O. Anal. Calcd. for $C_{39}H_{44}NO_{11}PRu$: C, 56.11; H, 5.31; N, 1.68. Found: 55.7; H, 5.26; N, 1.59. IR: $\tilde{v}/cm^{-1}$ = 3347m-br ($v_{OH} + v_{NH}$), 3063w, 2960w, 2926m, 2880w, 2857w, 1692m-sh; 1667s, 1650-1640s ($v_{C8=O} + v_{C17=O}$), 1552m, 1436m, 1392m, 1313m, 1164w, 1095m, 1078m, 1039m, 790w, 753w, 724w, 698m. ^1H NMR (CD₃OD): δ (ppm) = 7.83 (dd, $^3J_{HH}$ = 8.3 Hz, J_{HP} = 1.8 Hz, 2H, C15-H), 7.64–7.51 (m, 10H, Ph), 7.47 (dd, J_{HP} = 10.2 Hz, $^3J_{HH}$ = 8.5 Hz, 2H, C14-H), 5.75 (d, $^3J_{HH}$ = 5.5 Hz, 2H, C4-H), 5.45–5.41 (m, 2H, C3-H), 4.31 (d, $^3J_{HH}$ = 7.8 Hz, 1H, C20-H), 4.07–3.99 (m, 1H, C19-H), 3.85 (d, $^2J_{HH}$ = 11.9 Hz, 1H, C25-H), 3.81–3.74 (m, 1H, C19-H'), 3.72–3.66 (m, 1H, C18-H), 3.63 (dd, $^2J_{HH}$ = 11.9 Hz, $^3J_{HH}$ = 5.1 Hz, 1H, C25-H'), 3.58–3.50 (m, 1H, C18-H'), 3.36–3.33 (m, 1H, C22-H), 3.29–3.26 (m, 2H, C23-H + C24-H), 3.23–3.17 (m, 1H, C21-H), 2.60 (hept, $^3J_{HH}$ = 6.5 Hz, 1H, C6-H), 1.94 (s, 3H, C1-H), 1.23 (d, $^3J_{HH}$ = 6.9 Hz, 6H, C7-H). No changes were observed in the ^1H NMR spectrum after 48 h at room temperature. $^{13}C\{^1H\}$ NMR (CD₃OD): δ (ppm) = 169.4 (C17), 167.1 (C8), 138.2 (C16), 135.6 (d, $^2J_{CP}$ = 5 Hz, C10), 135.5 (d, $^2J_{CP}$ = 5 Hz, C10'), 135.2 (d, $^2J_{CP}$ = 10 Hz, C14), 134.1 (d, $^1J_{CP}$ = 43 Hz, C13), 132.8 (C12), 130.2 (d, $^3J_{CP}$ = 10 Hz, C11), 128.6 (d, $^3J_{CP}$ = 10 Hz, C15), 109.3 (d, $^2J_{CP}$ = 3 Hz, C5), 104.7 (C20), 99.4 (C2), 89.3 (t, $^2J_{CP}$ = 4 Hz, C4), 88.1 (t, $^2J_{CP}$ = 3 Hz, C3); 78.0, 77.9 (C22 + C23);

75.2 (C21), 71.6 (C24), 69.5 (C19), 62.7 (C25), 41.3 (C18), 32.3 (C6), 22.5 (C7), 18.1 (C1). ^{31}P{^{1}H}

NMR (CD$_3$OD): δ (ppm) = 32.4.

4. X-Ray crystallography.

Crystal data and collection details for [Ru(C$_2$O$_4$)(p-cymene)(H$_2$O)]·2H$_2$O are reported in Tables S2-S3.

Data were recorded on a Bruker APEX II diffractometer equipped with a PHOTON100 detector using

Mo–Kα radiation. Data were corrected for Lorentz polarization and absorption effects (empirical

absorption correction SADABS).[58] The structure was solved by direct methods and refined by full-

matrix least-squares based on all data using F^2.[59] Hydrogen atoms were fixed at calculated positions

and refined by a riding model, except those of the H$_2$O molecules, which were located on the Fourier

map and refined isotropically. All non-hydrogen atoms were refined with anisotropic displacement

parameters.

5. Behaviour of Ru complexes in aqueous media

Preliminary stability assessment in water/DMSO solution (NMR). The selected Ru compound was

dissolved a D$_2$O solution containing Me$_2$SO$_2$ ($3.5 \cdot 10^{-3}$ mol·L^{-1}); alternatively it was dissolved in

DMSO-d$_6$ and diluted with D$_2$O/Me$_2$SO$_2$. Appropriate D$_2$O/DMSO-d$_6$ v/v ratios were used,[38]

depending on the water solubility (0.7 mL total volume). The resulting yellow solution ($c_{Ru} \approx 5 \cdot 10^{-3}$

mol·L^{-1}) was maintained at 37 °C for 72 hours while periodically analysed by ^{1}H and ^{31}P{^{1}H} NMR. A

single set of signals was observed in ^{1}H and ^{31}P{^{1}H} NMR spectra of the freshly-prepared solution,

attributed to the starting material. NMR data and other details are given in the Supporting Information.

The % amount of starting material in solution with respect to the initial spectrum was calculated using

Me$_2$SO$_2$ as internal standard (Table S4).

Stability in cell culture medium (NMR, MS). The selected Ru compound was dissolved in DMSO

(0.25 mL) then diluted with RPMI-1640 cell culture medium (5 mL; 5% DMSO). The resulting yellow

solution ($c_{Ru} \approx 1.5 \cdot 10^{-3}$ mol·L^{-1}) was maintained at 37 °C for 72 hours and periodically sampled for ^{31}P{^{1}H} NMR (sealed C$_6$D$_6$ capillary for locking). Besides phosphate (δ = 2.4 ppm), only one signal was observed in the ^{31}P{^{1}H} NMR spectrum of the freshly-prepared solution, attributed to the starting material. In the case of **Ru2α** and **Ru2β**, no other ^{31}P NMR signal was clearly visible up to 72 h.

Workup #1 (**Ru2α**, **Ru2β**). Water (15 mL) was added and the mixture was extracted with CH$_2$Cl$_2$ (3x10 mL). The combined organic extracts were dried under vacuum (40 °C). The resulting yellow solid was analysed by ^{1}H and ^{31}P{^{1}H} NMR (CD$_3$OD) (Figures S55-S56). The % amount of starting Ru complex was calculated by ^{1}H NMR with respect to other identified species.

Workup #2 (**Ru3**, **Ru4**). Volatiles were removed under vacuum (40°C). The residue was suspended in MeCN (5 mL) and filtered over celite. The filtrate solution was taken to dryness under vacuum and the resulting yellow solid was analysed by ^{1}H and ^{31}P{^{1}H} NMR and ESI-MS(+) in CD$_3$OD. Mass spectrometry measurements in positive ion scan mode were performed with an API4000 instrument (SCIEX) equipped with an Ionspray/APCI source. In each case, the starting material was identified in the organic residue, together with other species. NMR, MS data and other details are given in the Supporting Information.

Speciation in methanol/water and interactions with small sulphur-containing biomolecules (MS).
Solutions of **Ru1α** and **Ru1β** (10 μM) in methanol/water 1:1 *v/v* were analysed immediately after the preparation and after 24 h by ESI+ mass spectrometry. The obtained ESI+MS spectra are given in Figures S58-S62. The interaction studies of the complexes with L-cysteine (cys) and glutathione (GSH) were performed in accordance with the previously published procedure[60] using the hyphenated HPLC-MS system composed of Agilent 1260 HPLC (Agilent Technologies) and Bruker amaZon SL ion trap spectrometer using the positive electrospray ionization (ESI+). MS spectra are given in Figures S63-S68.

6. Biological studies.

40

Cell viability assay using MTT test. Human cancer cell lines (A2780, A2780R, MCF7, HepG2, HOS, PC-3, A549, and HeLa), human fetal lung fibroblasts (MRC-5) and human embryonic kidney cells (HEK-293) were plated at 96-well dishes, using culture media supplemented with 10% of fetal calf serum and employing the conditions recommended by a supplier. Cells were incubated for 24 h with the tested compounds, vehicle (UT; 0.1% v/v DMF) and Triton X-100 (1%; v/v). Conventional MTT assay was performed and the absorbance (A) was measured spectrophotometrically at 570 nm on an Infinite M200 (Schoeller Instruments, Prague, Czech Republic). The data were expressed as the percentage of cell viability, where 100% and 0% represent the treatments with the negative control (DMF) and positive control (Triton X-100), respectively. Half-maximal inhibitory concentrations (IC$_{50}$) were calculated using GraphPad Prism 6 software (GraphPad Software, San Diego, USA).

Cell culture. For studying toxicity mechanism of **Ru1α** and **Ru1β**, the human ovarian cancer cell line A2780 (Sigma, 93112519-1VL) was cultured at 37 °C under a 5% CO$_2$ atmosphere in RPMI-1640 Medium (Sigma Aldrich, USA) supplemented with L-Glutamine (2 mM), fetal bovine serum (FBS, 10%), 5 U/mL penicillin and 50 µg /mL streptomycin).

Cell cycle analysis. The A2780 cells were treated with 15 µM of **Ru1α**, **Ru1β** or cisplatin for 24 h. After the incubation, the cells were washed with PBS (0.1 M, pH 7.4) and cell cycle analysis was performed according to the protocol of BD Cycletest^{TM} Plus DNA kit (Becton Dickinson, USA). The experiments were done in duplicates and at least $5*10^3$ events were recorded for each sample using BD FACSVerse flow cytometer (Becton Dickinson, USA).

Apoptosis analysis. Early/late stage of apoptosis was detected using Annexin V-FITC apoptosis detection kit (Enzo Life Sciences, USA). Caspase induction was determined by CellEvent^{TM} Caspase-3/7 Green Flow Cytometry Assay Kit (Thermo Fisher Scientific, USA). Both methods were done according to the manufacturer protocol with one modification in caspase induction, which was the use of only CellEvent^{TM} Caspase-3/7 Green Detection Reagent for detection of Caspase-3/7 activation. $50*10^3$ cells/well were seeded in 24-well plate and treated with 15 µM of **Ru1α**, **Ru1β** or cisplatin for

24 h next day. After incubation, the cells were washed once with PBS (0.1M, pH 7.4), detached with trypsin (0.25% in ethylenediaminetetraacetic acid (EDTA), Sigma-Aldrich), resuspended in 500 µL of culture medium. After staining with appropriate dyes, the measurements were performed in duplicates and at least $10*10^3$ events were recorded for each sample using BD FACSVerse flow cytometer (Becton Dickinson, USA).

Oxidative stress analysis. The A2780 cells were treated with 15 µM of **Ru1α**, **Ru1β** or cisplatin for 24 h. The oxidative stress analysis was performed using ROS-ID ® Total ROS/Superoxide detection kit (Enzo Life Sciences, USA) according to the manufacturer protocol. The samples were analyzed in triplicates on multimode microplate reader Infinite PRO M200 (Tecan, Switzerland).

Mitochondrial membrane potential (MMP) analysis. The A2780 cells were incubated with 15 µM **Ru1α**, **Ru1β** or cisplatin for 24 h. The cells were washed with PBS (0.1 M, pH 7.4), detached with trypsin (0.25% EDTA, Sigma-Aldrich), and resuspended in 500 µL of culture medium. The cells were stained with MITO-ID® Membrane potential detection kit (Enzo Life Sciences, USA) according to the manufacturer protocol and samples were measured the in duplicates, while at least $10*10^3$ events were recorded using BD FACSVerse flow cytometer (Becton Dickinson, USA).

Statistical analysis. For cell cycle, apoptosis, MMP and oxidative stress analysis, we performed three independent experiments and the mean ± standard deviation (SD) was calculated. One-way ANOVA was performed using Statistica software[44] and significant difference between samples was highlighted. Different letters indicate statistically significant differences at $p \leq 0.05$.

Cellular uptake. The A2780 cells were seeded in 6-well culture plates and incubated for 2, 6, 12, 24 and 48 h with **Ru1α**, **Ru1β** or cisplatin in concentrations corresponding to their IC_{50} values obtained for the 24 h incubation using the MTT test and left to interact with them. The cells were harvested by the trypsinization, centrifugated and cell pellets were digested with 500 µL of concentrated nitric acid for ICP-MS (65%, at 70 °C, overnight). Before the analysis, the solutions were diluted with 4.5 mL of ultrapure water for ICP-MS and the Ru content was determined by ICP-MS (ICP-MS spectrometer

7700x, Agilent) using the external calibration. The obtained values were corrected for adsorption effects.

Conflicts of interest.

There are no conflicts to declare.

Supporting Information Available

Solid-state IR and NMR spectra of compounds. X-ray data: structure of **Ru-H$_2$O.** Solution stability studies, interaction with biomolecules (NMR and MS data and spectra). CCDC reference number 2120282 contains the supplementary crystallographic data for the X-ray study reported in this paper. These data can be obtained free of charge at https://www.ccdc.cam.ac.uk/structures/ or from the Cambridge Crystallographic Data Centre, 12, Union Road, Cambridge CB2 1EZ, UK; e-mail: deposit@ccdc.cam.ac.uk.

References

1   E. J. Anthony, E. M. Bolitho, H. E. Bridgewater, O. W. L. Carter, J. M. Donnelly, C. Imberti, E. C. Lant, F. Lermyte, R. J. Needham, M. Palau, P. J. Sadler, H. Shi, F.-X. Wang, W.-Y. Zhang, Z. Zhang, Metallodrugs are unique: opportunities and challenges of discovery and development. Chem. Sci. 11 (2020) 12888–12917.

2   (a) E. Alessio, Thirty Years of the Drug Candidate NAMI-A and the Myths in the Field of Ruthenium Anticancer Compounds: A Personal Perspective. Eur. J. Inorg. Chem. (2017) 1549–1560. (b) R. Trondl, P. Heffeter, C. R. Kowol, M. A. Jakupec, W. Berger, B. K. Keppler, NKP-1339, the first ruthenium-based anticancer drug on the edge to clinical application, Chem. Sci. 5 (2014) 2925.

3   (a) B. S. Murray, P. J. Dyson, Recent progress in the development of organometallics for the treatment of cancer. Curr. Opinion Chem. Biol. 56 (2020) 28–34. (b) P. Zhang, P. J. Sadler, Advances in the design of organometallic anticancer complexes, J. Organomet. Chem. 839 (2017) 5-14. (c) L. Zeng, P. Gupta, Y. Chen, E. Wang, L. Ji, H. Chao, Z.-S. Chen, The development of anticancer ruthenium(II) complexes: from single molecule compounds to nanomaterials. Chem. Soc. Rev. 46 (2017) 5771-5804.

4   (a) B. S. Murray, M. V. Babak, C. G. Hartinger, P. J. Dyson, The development of RAPTA compounds for the treatment of tumors, Coord. Chem. Rev. 306 (2016) 86–114. (b) A. Weiss, D. Bonvin, R. H. Berndsen, E. Scherrer, T. J. Wong, P. J. Dyson, A. W. Griffioen, P. Nowak-Sliwinska, Angiostatic treatment prior to chemo- or photodynamic therapy improves anti-tumor efficacy, Sci. Rep. 5 (2014) 8990. (c) R. H. Berndsen, A. Weiss, U. Kulsoom Abdul, T. J. Wong, P. Meraldi, A. W. Griffioen, P. J. Dyson, P. Nowak-Sliwinska, Combination of ruthenium(II)-arene complex $[Ru(\eta^6$-p-cymene)Cl_2(pta)] (RAPTA-C) and the epidermal growth factor receptor inhibitor erlotinib results in efficient angiostatic and antitumor activity, Sci. Rep. 7 (2017) 43005.

5   (a) P. Štarha, Z. Trávníček, Non-platinum complexes containing releasable biologically active ligands. Coord. Chem. Rev. 395 (2019), 130-145. (b) R. G. Kenny, C. J. Marmion, Toward Multi-Targeted Platinum and Ruthenium Drugs-A New Paradigm in Cancer Drug Treatment Regimens? Chem. Rev. 199 (2019), 1058–1137. (c) A. Khoury, K. M. Deo, J. R. Aldrich-Wright, Recent advances in platinum-based chemotherapeutics that exhibit inhibitory and targeted mechanisms of action. J. Inorg. Biochem. 207 (2020), 111070. (d) E. Boros, P. J. Dyson, G. Gasser, Classification of Metal-based Drugs According to Their Mechanisms of Action. *Chem.* 6 (2020) 41-60.

6   G. Bononi, D. Iacopini, G. Cicio, S. Di Pietro, C. Granchi, V. Di Bussolo, F. Minutolo, Glycoconjugated Metal Complexes as Cancer Diagnostic and Therapeutic Agents, ChemMedChem 16 (2021) 30-64.

7   (a) S. Gomez, A. Tsung, Z. Hu, Current Targets and Bioconjugation Strategies in Photodynamic Diagnosis and Therapy of Cancer, Molecules 25 (2020), 4964. (b) K. J. Doores, D.. P. Gamblin, B. G. Davis, Exploring and Exploiting the Therapeutic Potential of Glycoconjugates, Chem. Eur. J. 12 (2006), 656-665. (c) C. G. Hartinger, A. A. Nazarov, S. M. Ashraf, P. J. Dyson, B. K. Keppler, Carbohydrate-Metal Complexes and their Potential as Anticancer Agents, Curr. Med. Chem. 15 (2008) 2574-2591. (d)

K.H. Thompson, C. Orvig, Design of targeting ligands in medicinal inorganic chemistry, Chem. Soc. Rev. 35 (2006) 534-544.

8   (a) E. C. Calvaresi, P. J. Hergenrother, Glucose conjugation for the specific targeting and treatment of cancer, Chem. Sci. 4 (2013) 2319-2333. (b) S. S. Pinho, C. A. Reis, Glycosylation in cancer: mechanisms and clinical implications. Nat. Rev. Cancer 15 (2015), 540–555.

9   M. I. Molejon, G. Weiz, J. D. Breccia, M. I. Vaccaro, Glycoconjugation: An approach to cancer therapeutics, World J. Clin. Oncol. 11 (2020), 110-120.

10   Selected references: (a) P. R. Florindo, D. M. Pereira, P. M. Borralho, C. M. P. Rodrigues, M. F. M. Piedade, A. C. Fernandes, Cyclopentadienyl–Ruthenium(II) and Iron(II) Organometallic Compounds with Carbohydrate Derivative Ligands as Good Colorectal Anticancer Agents, J. Med. Chem. 58 (2015), 4339–4347. (b) M. Patra, S. G. Awuah, S. J. Lippard, Chemical Approach to Positional Isomers of Glucose–Platinum Conjugates Reveals Specific Cancer Targeting through Glucose-Transporter-Mediated Uptake in Vitro and in Vivo, J. Am. Chem. Soc. 138 (2016) 12541–12551. (c) M. Patra, T. C. Johnstone, K. Suntharalingam, S. J. Lippard, A Potent Glucose–Platinum Conjugate Exploits Glucose Transporters and Preferentially Accumulates in Cancer Cells, Angew. Chem. Int. Ed. 55 (2016) 2550-2554. (d) L. N. Lameijer, S. L. Hopkins, T. G. Brevé, S. H. C. Askes, S. Bonnet, D- Versus L-Glucose Conjugation: Mitochondrial Targeting of a Light-Activated Dual-Mode-of-Action Ruthenium-Based Anticancer Prodrug, Chem. Eur. J. 22 (2016) 18484-18491. (e) J. Ma, X. Yang, W. Hao, Z. Huang, X. Wang, P. G. Wang, Mono-functionalized glycosylated platinum(IV) complexes possessed both pH and redox dual-responsive properties: Exhibited enhanced safety and preferentially accumulated in cancer cells in vitro and in vivo, Eur. J. Med. Chem. 128 (2017), 45-55. (f) A. Annunziata, D. Liberti, E. Bedini, M. E. Cucciolito, D. Loreto, D. M. Monti, A. Merlino, F. Ruffo, Square-Planar vs. Trigonal Bipyramidal Geometry in Pt(II) Complexes Containing Triazole-Based Glucose Ligands as Potential Anticancer Agents, Int. J. Mol. Sci. 22 (2021), 8704.

11   (a) N. K. Kochetkov, E. E. Nifantev, M. P.Koroteev, Z. K. Zhane, A. A. Borisenko, Synthesis and stereochemistry of 6-deoxy-6-halogeno-D-glucofuranose cyclic phosphates, Carbohydr. Res. 47 (1976) 221-231. (b) E. E. Nifantyev, M. P. Koroteev, A. M. Koroteev,V. K. Belsky, A. I. Stash, M. Yu. Antipin, K. A. Lysenko,L. Cao, Metal complexes based on monosaccharide bicyclophosphites as new available chiral coordination systems, J. Organomet. Chem. 587 (1999) 18–27.

12   (a) I. Berger, M. Hanif, A. A. Nazarov, C. G. Hartinger, R. O. John, M. L. Kuznetsov, M. Groessl, F. Schmitt, O. Zava, F. Biba, V. B. Arion, M. Galanski, M. A. Jakupec, L. Juillerat-Jeanneret, P. J. Dyson, B. K. Keppler, In Vitro Anticancer Activity and Biologically Relevant Metabolization of Organometallic Ruthenium Complexes with Carbohydrate-Based Ligands, Chem. Eur. J. 14 (2008) 9046–9057. (b) M. Hanif, S. M. Meier, W. Kandioller, A. Bytzek, M. Hejl, C. G. Hartinger, A. A. Nazarov, V. B. Arion, M. A. Jakupec, P. J. Dyson, B. K. Keppler, From hydrolytically labile to hydrolytically stable Ru^{II}–arene

anticancer complexes with carbohydrate-derived co-ligands, J. Inorg. Biochem. 105 (2011) 224–231. (c) M. Hanif, A. A. Nazarov, C. G. Hartinger, Synthesis of [Ru^{II}(η^6-*p*-cymene)(PPh$_3$)(L)Cl]PF$_6$ complexes with carbohydrate-derived phosphites, imidazole or indazole co-ligands, Inorg. Chim. Acta 380 (2012) 211–215. (d) M. Hanif, S. M. Meier, A. A. Nazarov, J. Risse, A. Legin, A. Casini, M. A. Jakupec, Bernhard K. Keppler, C. G. Hartinger, Influence of the π-coordinated arene on the anticancer activity of ruthenium(II) carbohydrate organometallic complexes, Front. Chem. 1 (2013) 27.

13   M. Böge, C. Fowelin, P. Bednarski, J. Heck, Diaminohexopyranosides as Ligands in Half-Sandwich Ruthenium(II), Rhodium(III), and Iridium(III) Complexes, Organometallics 34 (2015) 1507−1521.

14   J. P. Byrne, P. Musembia, M. Albrecht, Carbohydrate-functionalized N-heterocyclic carbene Ru(ii) complexes: synthesis, characterization and catalytic transfer hydrogenation activity, Dalton Trans. 48 (2019) 11838-11847.

15   I. Kacsir, A. Sipos, G. Ujlaki, P. Buglyó, L. Somsák, P. Bai, É. Bokor, Ruthenium Half-Sandwich Type Complexes with Bidentate Monosaccharide Ligands Show Antineoplastic Activity in Ovarian Cancer Cell Models through Reactive Oxygen Species Production, Int. J. Mol. Sci. 22 (2021), 10454.

16   M. Lamač, M. Horáček, L. Červenková Šťastná, J. Karban, L. Sommerová, H. Skoupilová, R. Hrstka, J. Pinkas, Harmless glucose-modified ruthenium complexes suppressing cell migration of highly invasive cancer cell lines, App. Organomet. Chem. 34 (2020), e5318.

17   (a) W. Szeja, P. Świerk, G. Grynkiewicz, A. Rusin, K. Papaj, An approach to C-glycosidic conjugates of isoflavones, Heterocycl. Comm. 19 (2013) 133-138. (b) A. Rusin, J. Zawisza-Puchałka, K. Kujawa, A. Gogler-Pigłowska, J. Wietrzyk, M. Świtalska, M. Głowala-Kosińska, A. Gruca, W. Szeja, Z. Krawczyk, G. Grynkiewicz, Synthetic conjugates of genistein affecting proliferation and mitosis of cancer cells, Bioorg. Med. Chem. 19 (2011), 295-305.

18   K. Polkowski, J. Popiołkiewicz, P. Krzeczyński, J. Ramza, W. Pucko, O. Zegrocka-Stendel, J. Boryski, J. S. Skierski, A. P. Mazurek, G. Grynkiewicz, Cytostatic and cytotoxic activity of synthetic genistein glycosides against human cancer cell lines, Cancer Lett. 203 (2004) 59-69.

19   (a) L. Biancalana, M. Gruchała, L. K. Batchelor, A. Błauż, A. Monti, G. Pampaloni, B. Rychlik, P. J. Dyson, F. Marchetti, Conjugating Biotin to Ruthenium(II) Arene Units via Phosphine Ligand Functionalization, Eur. J. Inorg Chem (2020) 1061-1072. (b) E. Păunescu, S. McArthur, M. Soudani, R. Scopelliti, P. J. Dyson, Nonsteroidal Anti-inflammatory—Organometallic Anticancer Compounds, Inorg. Chem. 55 (2016), 1788-1808. (c) Z. Kokan, B. Perić, G. Kovačević, A. Brozovic, N. Metzler-Nolte, S. I. Kirin, cis- versus trans-Square-Planar Palladium(II) and Platinum(II) Complexes with Triphenylphosphine Amino Acid Bioconjugates, Eur. J. Inorg. Chem. (2017) 3928-3937. (d) S. Tasan, O. Zava, B. Bertrand, C. Bernhard, C. Goze, M. Picquet, P. Le Gendre, P. Harvey, F. Denat, A. Casini, E. Bodio, BODIPY–phosphine as a versatile tool for easy access to new metal-based theranostics,

Dalton Trans. 42 (2013) 6102-6109. (e) P. Štarha, Z. Trávníček, Non-platinum complexes containing releasable biologically active ligands, Coord. Chem. Rev. 395 (2019) 130–145.

20   (a) V. Di Bussolo, M. Caselli, M. R. Romano, M. Pineschi, P. Crotti, Stereospecific Uncatalyzed α-O-Glycosylation and α-C-Glycosidation by Means of a New D-Gulal-Derived α Vinyl Oxirane. J. Org. Chem. 69 (2004) 7383-7386. (b) V. Di Bussolo, L. Checchia, M. R. Romano, M. Pineschi, P. Crotti, Stereoselective Synthesis of 2,3-Unsaturated 1,6-Oligosaccharides by Means of a Glycal-Derived Allyl Epoxide and N-Nosyl Aziridine Org. Lett. 10 (2008) 2493-2496. (c) V. Di Bussolo, I. Frau, L. Favero, G. Uccello-Barretta, F. Balzano, P. Crotti, Regio- and stereoselective behavior of l-arabinal-derived vinyl epoxide in nucleophilic addition reactions. Comparison with conformationally restricted d-galactal-derived analogs, Tetrahedron 71 (2015) 6276-6284. (d) D. Iacopini, G. Barbini, L. Favero, M. Pineschi, S. Di Pietro, V. Di Bussolo, Stereoselective synthesis of new pyran-dioxane based polycycles from glycal derived vinyl epoxide. Org. Biomol. Chem. 19 (2021) 9190-9198.

21   Since **VEα**, is prepared from **VEβ**, via 6-*O*-benzyl-D-gulal (see Scheme 1 and Ref. 20a), compounds with β stereochemistry precede those with α stereochemistry throughout the manuscript.

22   V. Di Bussolo, M. Caselli, M. R. Romano, M. Pineschi, P. Crotti, Regio- and Stereoselectivity of the Addition of O-, S-, N-, and C-Nucleophiles to the β Vinyl Oxirane Derived from d-Glucal, J. Org. Chem. 2004, 69, 25, 8702–8708.

23   V. Di Bussolo, E. C. Calvaresi, C. Granchi, L. Del Bino, I. Frau, M. C. Dasso Lang, T. Tuccinardi, M. Macchia, A. Martinelli, P. J. Hergenrother, F. Minutolo, Synthesis and biological evaluation of non-glucose glycoconjugated N-hydroxindole class LDH inhibitors as anticancer agents, RSC Adv. 5 (2015) 19944.

24   D. Hérault, D. H. Nguyen, D. Nuela, G. Buono, Reduction of secondary and tertiary phosphine oxides to phosphines, Chem. Soc. Rev. 44 (2015) 2508-2528.

25   (a) M. A. Hyland, M. D. Morton, C. Brückner, meso-Tetrakis(pentafluorophenyl)porphyrin-Derived Chromene-Annulated Chlorins. J. Org. Chem. 77 (2012) 3038–3048. (b) W.-C. Yeo, J. J. Vittal, L. L. Koh, G. K. Tan, P.-H. Leung, Functionalization of Metal-Protected Chiral Phosphines via Simple Organic Transformations. Organometallics 25 (2006) 1259–1269. (c) V. E. Zottig, M. A. Todd, A. C. Nichols-Nielander, D. P. Harrison, M. Sabat, W. H. Myers, W. Dean Harman, Epoxidation, Cyclopropanation, and Electrophilic Addition Reactions at the meta Position of Phenol and meta-Cresol. Organometallics 29 (2010) 4793–4803. (d) M. D. Levin, T. Q. Chen, M. E. Neubig, C. M. Hong, C. A. Theulier, I. J. Kobylianskii, M. Janabi, J. P. O'Neil, F. Dean Toste, A catalytic fluoride-rebound mechanism for C(sp3)-CF3 bond formation. Science 356 (2017) 1272-1276. (e) A. J. Pearson, Eugen F. Mesaros, Stereocontrolled Construction of Tetrahydrofurans and γ-Butyrolactones Using Organomolybdenum Chemistry. Org. Lett. 3 (2001) 2665–2668. (f) M. Gómez, N. Rendón, E. Álvarez, K. Mereiter, M. L. Poveda, M. Paneque, Functionalization of 3-Iridacyclopentenes. Chem. Eur. J. 23

(2017) 16346-16356. (g) A. J. Pearson, M. K. Manoj Babu, Reactions of Alkyllithium and Grignard Reagents with (Cyclopentadienyl)dicarbonyl(2-methylbutadiene)molybdenum: Observations of Solvent Effects on Regioselectivity. Organometallics 13 (1994) 2539–2541.

26   (a) O. Neunhoeffer, L. Lamza, Diphenyl-[p-hydroxy-phenyl]-phosphin-β-D-glucosid, Chem. Ber. 96 (1961) 2519-2521. (b) T. N. Mitchell, K. Heesche-Wagner, Approaches to new water-soluble phosphines, J. Organomet. Chem. 436 (1992) 43-53. (c) M. Beller, J. G. E. Krauter, A. Zapf, Carbohydrate-substituted triarylphosphanes-a new class of ligands for two-phase catalysis, Angew. Chem., Int. Ed. 36 (1997), 772-774. (d) M. Beller, J. G. E. Krauter, A. Zapf, S. Bogdanovic; Carbohydrate-substituted phosphines as new ligands for two-phase catalysis - synthesis and application, Cat. Today 48 (1999) 279–290. (e) H. Brunner, M. Schonherr, M. Zabel, Enantioselective catalysis. Part 142: Carbohydrate-derived oxime ethers from functionalised aldehydes and O-β-D-glucopyranosylhydroxylamine—new C=N ligands stable towards hydrolysis, Tetrahedron: Asymmetry 12 (2001) 2671–2675. (f) H. Brunner, M. Schonherr, M. Zabel, Enantioselective catalysis. Part 148: Carbohydrate-derived oxime ethers stable towards hydrolysis—syntheses of ligands and complexes and a study of their catalytic properties, Tetrahedron: Asymmetry 14 (2003) 1115–1122. (g) R. S. Loka, C. M. Sadek, N. A. Romaniuk, C. W. Cairo, Conjugation of Synthetic N-Acetyl-Lactosamine to Azide-Containing Proteins Using the Staudinger Ligation, Bioconjugate Chem. 21 (2010) 1842–1849. (h) W. Ndugire, B. Wu, M. Yan, Synthesis of carbohydrate-grafted glycopolymers using a catalyst-free, perfluoroarylazide-mediated fast staudinger reaction Molecules 24 (2019) 157/1-157/11.

27   (a) S. Hanessian, Preparative Carbohydrate Chemistry (1997) 283-285. (b) F. D'Andrea, G. Vagelli, C. Granchi, L. Guazzelli, T. Tuccinardi, G. Poli, D. Iacopini, F. Minutolo, V. Di Bussolo, Synthesis and Biological Evaluation of New Glycoconjugated LDH Inhibitors as Anticancer Agents, Molecules 24 (2019) 3520

28   (a) A. V. Demchenko in "Handbook of Chemical Glycosylation: Advances in Stereoselectivity and Therapeutic Relevance" 1°Ed. (2008) Wiley-VCH. (b) B. K. Gorityala, Z. Lu, M. L. Leow, J. Ma, X. Liu, In Vivo and in Situ Tracking Cancer Chemotherapy by Highly Photostable NIR Fluorescent Theranostic Prodrug. J. Am. Chem. Soc. 134 (2012) 15229-15232.

29   (a) S. di Pietro, V. Bordoni, D. Iacopini, S. Achili, M. Pineschi, M. Thépaut, F. Fieschi, P. Crotti, V. Di Bussolo, New lipophilic glycomimetic DC-SIGN ligands: Stereoselective synthesis and SPR-based binding inhibition assays, Bioorg. Chem. 107 (2021) 104566. (b) V. Bordoni, V. Porkolab, S. Sattin, M. Thépaut, I. Frau, L. Favero, P. Crotti, A. Bernardi, F. Fieschi, V. Di Bussolo, Stereoselective innovative synthesis and biological evaluation of new real carba analogues of minimal epitope Manα(1,2)Man as DC-SIGN inhibitors, RSC Adv., 2016,6, 89578-89584

30   A. K. Sanki, L. K. Mahal, A One-Step Synthesis of Azide-Tagged Carbohydrates: Versatile -Intermediates for Glycotechnology, Synlett (2006) 455–459.

31   M. Ohff, J. Holz, M. Quirmbach, A. Börner, Borane Complexes of Trivalent Organophosphorus Compounds. Versatile Precursors for the Synthesis of Chiral Phosphine Ligands for Asymmetric Catalysis, Synthesis (Stuttg). 10 (1998) 1391–1415.

32   NMR purity = 95% ; see details in the experimental section.

33   (a) L. Palais, I. S. Mikhel, C. Bournaud, L. Micouin, C. A. Falciola, M. Vuagnoux-d'Augustin, S. Rosset, G. Bernardinelli, A. Alexakis, SimplePhos Monodentate Ligands: Synthesis and Application in Copper-Catalyzed Reactions. Angew. Chem. Int. Ed. 46 (2007) 7462 –7465.

34   (a) N. Brodie, S. Juge, Phosphine Boranes in Coordination Chemistry: An Efficient Method for the Synthesis of Chiral and Achiral Organophosphorus Pentacarbonyltungsten Complexes. Inorg. Chem. 37 (1998) 2438-2442. (b) C. Darcel, E. B. Kaloun, R. Merdes, D. Moulin, N. Riegel, S. Thorimbert, J. P. Genet, S. Juge, Direct use of chiral or achiral organophosphorus boranes as pro-ligands for transition metal catalyzed reactions. J. Organomet. Chem. 624 (2001) 333–343.

35   Selected recent references: (a) Z. Wu, P. Retailleau, V. Gandon, A. Voituriez, A. Marinetti, Use of Planar Chiral Ferrocenyl-phosphine-Gold(I) Complexes in the Asymmetric Cycloisomerization of 3-Hydroxylated 1,5-Enynes. Eur. J. Org. Chem. (2016) 70–75. (b) J. N. Smith, J. M. Hook, N. T. Lucas, Superphenylphosphines: Nanographene-Based Ligands That Control Coordination Geometry and Drive Supramolecular Assembly. J. Am. Chem. Soc. 140 (2018) 1131−1141. (c) S. Lapointe, E. Khaskin, R. R. Fayzullin, J. R. Khusnutdinova, Stable Nickel(I) Complexes with Electron-Rich, Sterically-Hindered, Innocent PNP Pincer Ligands. Organometallics 38 (2019) 1581-1594. (d) R. Konrath, A. Spannenberg, P. C. Kamer, Preparation of a Series of Supported Nonsymmetrical PNP-Pincer Ligands and the Application in Ester Hydrogenation. Chem. Eur. J. 25 (2019) 15341-15350.

36   A related intramolecular example is represented by [RuCl$_2$(η^6-p-cymene)(κP-PPh$_2$CH$_2$CH$_2$PPh$_2$BH$_3$)], showing ^{31}P NMR resonances at 23.6 (Ru−P) and 18.2 (B−P) ppm. A. B. Chaplin, R. Scopelliti, P. J. Dyson. The Synthesis and Characterisation of Bis(phosphane)-Linked (η6-p-Cymene)-ruthenium(II)–Borane Compounds, Eur. J. Inorg. Chem. (2005) 4762–4774.

37   Note that the p-cymene ligand is in free rotation around the metal-centroid axis at room temperature. (a) R. Baldwin, M. A. Bennett, D. C. R. Hockless, P. Pertici, A. Verrazzani, G. Uccello Barretta, F. Marchetti, P. Salvadori, Synthesis, structures and dynamic NMR spectra of η6-hexaethylbenzene complexes of ruthenium(0) and ruthenium(ii). J. Chem. Soc., Dalton Trans., 2002, 4488–4496. (b) R. K. Pomeroy, D. J. Harrison, Restricted Rotation of the Arene Ring in (p-Bu$^t_2$C$_6$H$_4$)Ru(CO)(SiCl$_3$)$_2$ J. Chem. Soc., Chem. Commun. (1980) 661-663.

38   The DMSO/water ratio was selected according to the solubility of the compounds in water; the organic co-solvent is needed to attain suitable concentration for a good quality ^{1}H NMR spectrum.

39   L. Biancalana, G. Ciancaleoni, S. Zacchini, A. Monti, F. Marchetti, G. Pampaloni, Solvent-Dependent Hemilability of (2-Diphenylphosphino)Phenol in a Ru(II) para-Cymene System. Organometallics 37 (2018) 1381-1391.

40   (a) A. Ashraf, F. Aman, S. Movassaghi, A. Zafar, M. Kubanik, W. Ahmad Siddiqui, J. Reynisson, T. Söhnel, S. M. F. Jamieson, M. Hanif, C. G. Hartinger, Structural Modifications of the Antiinflammatory Oxicam Scaffold and Preparation of Anticancer Organometallic Compounds, Organometallics 38 (2019) 361–374. (b) G. Kalaiarasi, M. Mohamed Subarkhan, F. Safwana, S. Sruthi, T. Sathiya Kamatchi, B. Keerthana, S. L. Ashok Kumar, New organoruthenium(II) complexes containing N, X-donor (X = O, S) heterocyclic chelators: Synthesis, spectral characterization, in vitro cytotoxicity and apoptosis investigation, Inorg. Chim. Acta 535 (2022) 120863.

41   L. H. Swift, R. M. Golsteyn, Cytotoxic amounts of cisplatininduce either checkpoint adaptationor apoptosis in a concentration-dependent manner in cancer cells. Biol. Cell 108 (2016) 127–148.

42   L. Galluzzi, L. Senovilla, I. Vitale, J. Michels, I. Martins, O. Kepp, M. Castedo, G. Kroemer, Molecular mechanisms of cisplatin resistance. Oncogene 31 (2012) 1869–1883.

43   V. Velma, S. R. Dasari, T. B. Tchounwou, Low Doses of Cisplatin Induce Gene Alterations, Cell Cycle Arrest, and Apoptosis in Human Promyelocytic Leukemia Cells, Biomark. Insights. 11 (2016) 113–121.

44   G. S. Salvesen, Caspases: opening the boxes and interpreting the arrows. Cell Death Differ. 9 (2002) 3–5. doi:10.1038/sj.cdd.4400963.

45   S. V. Winter, A. Zychlinsky, The bacterial pigment pyocyanin inhibits the NLRP3 inflammasome through intracellular reactive oxygen and nitrogen species, J. Biol. Chem. 293 (2018) 4893–4900.

46   Jayakumar, T.; Sheu, J.-R.; Hsia, C.-W.; Bhavan, P.S.; Chang, C.-C. Anti-Inflammatory Mechanisms of Novel Synthetic Ruthenium Compounds. Appl. Sci. 11 (2021) 10092.

47   Devagi, G., Mohankumar, A., Shanmugam, G. et al. Organoruthenium(II) Complexes Ameliorates Oxidative Stress and Impedes the Age Associated Deterioration in Caenorhabditis elegans through JNK-1/DAF-16 Signalling. Sci. Rep. 8 (2018) 7688 (2018).

48   W. Li, G.-B. Jiang, J.-H. Yao, X.-Z. Wang, J. Wang, B.-J. Han, Y.-Y. Xie, G.-J. Lin, H.-L. Huang, Y.-J. Liu, Ruthenium(II) complexes: DNA-binding, cytotoxicity, apoptosis, cellular localization, cell cycle arrest, reactive oxygen species, mitochondrial membrane potential and western blot analysis, J. Photochem. Photobiol. B 140 (2014) 94-104.

49   S. Bhattacharyya, K. Purkait, A. Mukherjee, Ruthenium(II) p-cymene complexes of a benzimidazole-based ligand capable of VEGFR2 inhibition: hydrolysis, reactivity and cytotoxicity studies, Dalton Trans. 46 (2017) 8539-8554.

50   (a) M. A. Bennett, A. K. Smith, Arene ruthenium(II) complexes formed by dehydrogenation of cyclohexadienes with ruthenium(III) trichloride. J. Chem. Soc., Dalton Trans. (1974) 233-241. (b) Optimized procedure: L. Biancalana, G. Pampaloni, S. Zacchini, F. Marchetti. Synthesis,

characterization and behavior in water/DMSO solution of Ru(II) arene complexes with bioactive carboxylates. J. Organomet. Chem. 869 (2018) 201-211.

51   G. R. Fulmer, A. J. M. Miller, N. H. Sherden, H. E. Gottlieb, A. Nudelman, B. M. Stoltz, J. E. Bercaw, K. I. Goldberg, NMR Chemical Shifts of Trace Impurities: Common Laboratory Solvents, Organics, and Gases in Deuterated Solvents Relevant to the Organometallic Chemist Organometallics 29 (2010) 2176–2179.

52   R. K. Harris, E. D. Becker, S. M. Cabral De Menezes, R. Goodfellow, P. Granger, NMR nomenclature. Nuclear spin properties and conventions for chemical shifts (IUPAC Recommendations 2001), Pure Appl. Chem. 73 (2001) 1795–1818.

53   V. Di Bussolo, M. Caselli, M. Pineschi, P. Crotti, New Stereoselective β-Glycosylation via a Vinyl Oxirane Derived from d-Glucal. Org. Lett. 4 (2002) 3695–3698.

54   A. V. Demchenko, Handbook of Chemical Glycosylation: Advances in Stereoselectivity and Therapeutic Relevance (2008) Wiley-VCH Verlag GmbH & Co. KGaA.

55   A. Staubitz, A. P. M. Robertson, M. E. Sloan, I. Manners, Amine− and Phosphine−Borane Adducts: New Interest in Old Molecules. Chem. Rev. 110 (2010) 4023–4078

56   W. H. Ang, E. Daldini, C. Scolaro, R. Scopelliti, L. Juillerat-Jeannerat, P. J. Dyson, Development of organometallic ruthenium-arene anticancer drugs that resist hydrolysis. Inorg. Chem. 45 (2006) 9006-9013.

57   The compound is best used when freshly-prepared. When stored in air for weeks, it turns dark yellow and less reactive. The pure compound can be recovered by suspending this solid in boiling water until a clear yellow solution is obtained.

58   G. M. Sheldrick, SADABS-2008/1 - Bruker AXS Area Detector Scaling and Absorption Correction, Bruker AXS: Madison, Wisconsin, USA, 2008.

59   G. M. Sheldrick, Crystal structure refinement with SHELXL. ActaCryst. C 71 (2015) 3.

60   R. Křikavová, J. Vančo, Z. Trávníček, J. Hutyra, Z. Dvořák, Design and characterization of highly in vitro antitumor active ternary copper(II) complexes containing 2′-hydroxychalcone ligands, Journal of Inorganic Biochemistry 163 (2016) 8–17.